

# **In BRAF<sup>V600E</sup>-mutated colorectal cancer cells, fascin1 restructures adherens junctions to drive Wnt activation.**

Eric Pham<sup>1\*</sup>, Amin Esmaeilniakooshkghazi<sup>1\*</sup>, Sudeep P. George<sup>1</sup>, Afzal Ahrorov<sup>1</sup>, Fabian R. Villagomez<sup>1</sup>, Michael Byington<sup>4</sup>, Srijita Mukhopadhyay<sup>2</sup>, Srinivas Patnaik<sup>1,3</sup>, Jacinta C. Conrad<sup>4</sup>, Monali Naik<sup>1</sup>, Saathvika Ravi<sup>1</sup>, Niall Tebbutt<sup>5</sup>, Jennifer Mooi<sup>5</sup>, Camilla M Reehorst<sup>5</sup>, John M. Mariadason<sup>5</sup>, Seema Khurana<sup>1,6@</sup>

<sup>1</sup> Department of Biology and Biochemistry, University of Houston, Houston TX 77204

<sup>2</sup> Department of Biology and Biochemistry, Center for Nuclear Receptors and Cell Signaling, University of Houston, Houston 77204, TX

<sup>3</sup> Current address: School of Biotechnology Campus XI, KIIT University, Bhubaneswar, Odisha 751024, India

<sup>4</sup> Department of Chemical and Biomolecular Engineering, University of Houston, Houston TX 77204

<sup>5</sup> Gastrointestinal Cancers Programs, Olivia Newton-John Cancer Research Institute, and La Trobe University School of Cancer Medicine, Melbourne, Victoria, Australia

<sup>6</sup> School of Allied Health Sciences, Baylor College of Medicine, Houston TX 77030

***Correspondence and requests for materials should be addressed to:*** Seema

Khurana, Ph.D., Department of Biology and Biochemistry, 369 Science and Research

Building SR2, Room 421E, 3455 Cullen Blvd., Houston, Texas 77004. E-mail:

[skhurana@central.uh.edu](mailto:skhurana@central.uh.edu); Tel: 713-743-2705.

**\* Both authors contributed equally to this manuscript.**

## Summary

Almost one-third of colorectal carcinomas (CRCs) arise from sessile serrated lesions (SSLs) which have > 90% rate of *BRAF*<sup>V600E</sup> mutations. Serrated pathway CRCs are aggressive, have poor prognosis and lack treatment options. The pro-metastasis actin-bundling protein fascin1 is absent from the normal colon but is a marker of SSLs and is differentially expressed between serrated pathway and conventional CRCs. However, its function in serrated pathway carcinogenesis has not been directly evaluated. We identify for the first time, the novel function of fascin1 in remodeling cell-cell adhesions in *BRAF*<sup>V600E</sup>-mutated CRC cells. Our study shows in *BRAF*<sup>V600E</sup>-mutated CRC cells fascin1 remodels adherens junction (AJ) mechanotransduction to directly activate oncogenic Wnt signaling which drives primary and secondary tumor growth in mice. More importantly, fascin1's AJ remodeling function contributes to the hybrid epithelial-mesenchymal (E/M) state and promotes collective cell migration. We identify fascin1 as a driver and a novel therapeutic target in serrated/*BRAF*<sup>V600E</sup>-mutated CRCs.

**Key Words:** Fascin1; serrated neoplasia pathway; aberrant Wnt signaling.

## Introduction

While the adenoma-carcinoma pathway is the major contributor to sporadic CRCs, evidence accumulated over the last decade shows that approximately 35% of CRCs arise *via* the alternative serrated pathway. Tumors arising *via* this pathway are enriched for the CpG island hypermethylation phenotype (CIMP), microsatellite instability (MSI), and mutations in the *BRAF* or *KRAS* oncogene.(De Sousa et al., 2013) These tumors arise from sessile serrated lesions (SSLs; hitherto called sessile serrated adenomas/polyps) and >90% of these lesions contain a *BRAF*<sup>V600E</sup> mutation.(Chen et al., 2021; De Sousa *et al.*, 2013) While ~35% of CRCs arise from precursor lesions with serrated glands, <10% of CRCs manifest a serrated morphology at diagnosis and a marker for all serrated pathway CRCs that arise from SSLs is lacking.<sup>2</sup> *BRAF*<sup>V600E</sup> mutation occurs early, is highly correlated with the serrated pathway, and defines a sub-population associated with a more aggressive disease course, reduced progression-free and overall survival, and treatment resistance. (Chen *et al.*, 2021; Pai et al., 2012) While selective inhibitors of *BRAF*<sup>V600E</sup> have been successfully used to treat metastatic melanomas these agents have minimal benefit as single agents in refractory *BRAF*<sup>V600E</sup> metastatic CRCs. Although recent studies have shown that this resistance can be partially overcome by combining BRAF inhibitors with epidermal growth factor receptor (EGFR) inhibitors, still only a subset of patients benefit, underscoring the critical need to find new treatments with better clinical outcomes for these patients.(Kopetz et al., 2015; Kopetz et al., 2019) The underlying genes that drive serrated pathway carcinogenesis remain unidentified, although, the *BRAF*<sup>V600E</sup> mutation has been linked to profound morphological changes including

dedifferentiation, cytoskeletal remodeling and disruption of adherens junctions (AJs) and tight junctions (TJs). (Conesa-Zamora et al., 2013; Herr et al., 2015; Makrodouli et al., 2011; Reischmann et al., 2020) While these changes are implicated in serrated pathway carcinogenesis, how these phenotypic changes influence tumorigenesis or the molecular mechanism responsible for these phenotypic changes are also not known. Identifying and understanding the role of these novel genes is, however, crucial in designing management approaches and therapies for serrated pathway CRCs.

Fascin1 is absent from the normal adult epithelium but is expressed in a wide range of carcinomas where its expression correlates with a clinically aggressive disease with a higher incidence of metastasis and poor prognosis. (Tan et al., 2013) In these carcinomas, fascin1 is both a driver and a prognostic indicator of metastatic disease. (Li et al., 2014) In multivariate analysis, fascin1 has been identified as an independent factor for CRCs, and fascin1 positive CRCs exhibit a greater ability to invade lymph nodes and develop extra-nodal tumor extensions, and have a higher likelihood of recurrence with a lower rate of disease-free and overall survival. (Hashimoto et al., 2006; Ristic et al., 2021; Tampakis et al., 2021) It is generally assumed that fascin1 drives tumor cell migration and invasion by assembling filopodia and invadopodia. However, there is emerging evidence that fascin1 also has cell migration-independent functions linked to tumor cell proliferation, oncogenesis, metastatic colonization, anoikis resistance, chemoresistance, and cancer stemness although the molecular mechanism underlying these non-canonical functions of fascin1 remain unclear. (Barnawi et al., 2016; Li et al., 2014; Ristic et al., 2021) Consequently, the mechanism by which fascin1 contributes to metastasis of CRCs remains unknown. Fascin1 is significantly upregulated in SSLs (~12 fold) and is identified

as a marker of SSLs.(Ashktorab et al., 2019; Kanth et al., 2019; Kanth et al., 2016) A recent study by Chen *et al* where single cell RNA-Seq was employed to investigate conventional and serrated polyps/adenomas revealed that fascin1 is significantly upregulated in serrated specific cells validating earlier reports that fascin1 is a marker of SSLs.(Chen *et al.*, 2021) Conesa-Zamora *et al* reported that fascin1 and hippocalcin are the two most differentially expressed genes between serrated adenocarcinomas and conventional CRCs.(Conesa-Zamora *et al.*, 2013) They also reported that fascin1 expression was associated with shorter survival which has been reported previously in CRCs.(Conesa-Zamora *et al.*, 2013; Hashimoto *et al.*, 2006) While these earlier works suggest that fascin1 could be a unique marker of serrated pathway CRCs and that it plays a critical role in serrated pathway carcinogenesis the function of fascin1 in the etiology of CRCs has not been directly investigated and its role in tumors arising *via* the serrated/*BRAF*<sup>V600E</sup> mutant pathway remains unknown.

Abnormal Wnt activation is a common feature of SSLs and serrated pathway CRCs, and early changes in Wnt signaling are linked to disease progression and poor prognosis.(Wu et al., 2008; Yachida et al., 2009) Elevated Wnt signaling is also common to the two known genetic mouse models of serrated CRC.(Tong et al., 2017) Nonetheless, unlike conventional CRCs, the molecular mechanism regulating aberrant Wnt activation in SSLs, serrated CRCs and CRCs with *BRAF*<sup>V600E</sup> mutation remains unidentified. In the absence of Wnt ligands, mechanical forces that change AJ mechanotransduction are sufficient to promote nuclear accumulation of  $\beta$ -catenin to drive Wnt target genes, and in this fashion they induce mechanical-strain induced changes in epithelial cell behavior.(Benham-Pyle et al., 2015) Wnt activation in response to changes in AJ

mechanotransduction plays an important role during morphogenesis and in tumorigenesis when these conserved embryonic mechanosensitive pathways are reactivated in the adult tissue.(Fernandez-Sanchez et al., 2015; Whitehead et al., 2008) Here we demonstrate, for the first time, that in *BRAF*<sup>V600E</sup> mutant CRCs, fascin1 remodels AJ mechanotransduction pathways to drive oncogenic Wnt activation. Our study also identifies fascin1 as a novel therapeutic target which has significant potential as a treatment for *BRAF*<sup>V600E</sup>-mutated CRCs and could significantly improve disease-free and overall survival.

## Results

***Fascin1 is upregulated in CRCs of the serrated pathway.*** Serrated pathway CRCs are a new subtype of CRCs that are associated with a worse prognosis than conventional CRCs. Fascin1 has been identified as a marker of SSLs.(Kanth *et al.*, 2019; Kanth *et al.*, 2016) A decade ago, Conesa-Zamora *et al* reported that in a CRC cohort of 70 fascin1 was one of two most differentially expressed gene between serrated adenocarcinomas and conventional CRCs that was also associated with shorter survival.(Conesa-Zamora *et al.*, 2013) Despite that to date the functional characterization of fascin1 in serrated pathway carcinogenesis remains uninvestigated. We analyzed fascin1 expression in a large cohort of 299 stage IV CRCs, from patients who participated in the Phase III MAX clinical trial.(Tebbutt et al., 2010) Analysis of fascin1 expression using the Hashimoto *et al* scoring criteria revealed low to high fascin1 expression in 34.4% of cases (score 1-3) while 22.4% of cases expressed moderate to high fascin1 protein levels (score 2-3; Fig 1A).(Hashimoto *et al.*, 2006) Notably, of the 5 serrated adenocarcinomas in this cohort 3

(60%) expressed high fascin1 (score 2-3). Furthermore, of the 23 *BRAF*<sup>V600E</sup> tumors in this cohort 14 (60.87%) expressed high levels of fascin1 (score 2-3), representing a statistically significant enrichment of fascin1 protein in this subgroup (P=0.0002, Fisher's exact test; Fig 1B). Fascin1 was also more highly expressed in high grade/poorly differentiated CRCs (G1>G2>G3; Supplementary Fig 1A).

***Fascin1 remodels adherens junctions and assembles tumor microtubule-like cell-cell junctions in *BRAF*<sup>V600E</sup> CRC cells.*** To identify the functional role of fascin1 in the pathogenesis of tumors arising *via* the serrated/*BRAF*<sup>V600E</sup> pathway, we performed knockdown (KD) studies of fascin1 in *BRAF*<sup>V600E</sup> mutant HT-29/19A CRC cells. Fascin1 targeting shRNA markedly reduced endogenous fascin1 protein expression in the parental cell line but did not affect EGFP-Fascin1 overexpression confirming on-target specificity of the shRNA constructs (Supplementary Fig 2A). Spheroids of HT-29/19A cells expressing scrambled shRNA (HT-29/19A-Scr) grew as loosely aggregated clusters of cells with a 'grape-like morphology.' Comparatively, fascin1 KD cells (HT-29/19A-shF) formed tightly organized, compact spheres (Fig 1C), implicating a role for fascin1 in the remodeling of cell-cell adhesions. In sub-confluent cell cultures, HT-29/19A-Scr cells formed nascent cell-cell adhesions that appeared as long filopodia-like protrusions that morphed into lamellipodia-like structures at the distal ends as two cells established cell-cell contact (Fig 1D). In contrast, HT-29/19A-shF cells extended much smaller lamellipodial protrusions as two cells approached each other, similar to nascent adherens junction (nAJ) assembly by normal epithelial cells.(Baum and Georgiou, 2011) Notably, Scr cells formed these protrusions even in the absence of direct cell-cell contact

(Supplementary Fig 2B). Alternatively, Scr cells formed long intercellular conduits that lack lamellipodia-like distal ends (Fig 1E). These remodeled cell-cell junctions contained fascin1, F-actin and tubulin (Figs 1D-1E) as well as E-cadherin demonstrating that these protrusions are indeed nAJs (Fig 1F). In these nAJs, fascin1 localized to both the filopodia-like and lamellipodia-like protrusions. By measuring the rate of assembly, we determined that fascin1, F-actin and tubulin are required to assemble these nAJs (Supplementary Figs 2C-2D). In normal epithelial cells AJs are assembled by a symmetrical 'push and pull' mechanism.(Krendel et al., 1999) Remarkably, fascin1 expressing Scr cells assemble AJs asymmetrically, where only one cell extends the protrusion (Cell 1, Fig 2A) with a lamellipodia-like distal end (red arrowhead) or long intercellular conduits (cyan arrowhead) while the neighboring cell assembles oblique actin bundles that attach to the E-cadherin and  $\beta$ -catenin foci (white arrowheads). In contrast, shF cells assemble AJs symmetrically where both cells generate similar protrusions and with the actin bundles in both cells arranged parallel to the plasma membrane. EGFP tagged fascin1 overexpressed in the non-transformed epithelial cells, MDCK (Supplementary Fig 2E) also results in the assembly of the ultra-long nAJs seen in HT-29/19A cells (Figs 2B). Notably, some MDCK EGFP-Fascin1 cells also initiated nAJ assembly by forming protrusions that resembled the sprouting phenotype of endothelial cells undergoing anastomosis (Fig 2C); or had a growth cone-like morphology (Fig 2D). More remarkably, these ultra-long nAJs contained functional mitochondria and lysosomes (Fig 2E).

These ultra-long AJs also formed in confluent cultures connecting two non-adjacent and significantly distant cells (Fig 3A, cell 1 is connected to cell 6). These remodeled AJs

hover over the confluent monolayer, which permits two distant cells to connect in this manner (Fig 3B). To analyze how fascin1 remodels ‘mature’ AJs, small clusters of MDCK EGFP and MDCK EGFP-Fascin1 cells were stimulated with hepatocyte growth factor (HGF) at concentrations that do not induce epithelial cell scatter. While the MDCK EGFP cells maintained cell-cell adhesions similar to normal epithelial cell clusters with few short-lived changes (Supplementary Video 1, Fig 3C), the MDCK EGFP-Fascin 1 cells continuously remodeled their cell-cell adhesions, dissolving and reforming them resulting in loosely connected cell clusters (Supplementary Video 2, Fig 3C). These dynamically remodeled cell-cell adhesions differed in length and lifespan which were positively correlated (Fig 3D). Morphologically similar structures called tunneling nanotubes are short-lived intercellular bridges with lifespans shorter than 60 min while tumor microtubes (TMs) are intercellular junctions with lifespans greater than 60 min.(Osswald et al., 2015; Rustom et al., 2004) Based on the morphological characteristics of the intercellular junctions between EGFP-Fascin1 cells and their lifespan of greater than 60 min, we refer to these remodeled cell-cell adhesions as tumor microtube-like (TM-like) cell-cell junctions rather than tunneling nanotube-like (TNT-like) intercellular junctions. It is noteworthy that fascin1 is expressed in astrocytomas and glioblastomas although fascin1’s role in the assembly of TMs in these cancers has not been studied.

***Fascin1 transforms adherens junction mechanotransduction in BRAF<sup>V600E</sup> CRC cells.*** In epithelial cells, the actin cytoskeleton is important for the stabilization of AJs, but it is also the force-generating mechanism that is required for AJ remodeling and it regulates AJ mechanotransduction.(Hoffman and Yap, 2015; Michael and Yap, 2013;

Schnittler et al., 2014) In normal epithelial cells, mature AJs are stable, continuous, and associated with actin bundles that are arranged parallel to the plasma membrane.(Yonemura, 2011) Fascin1 expressing mutant *BRAF* HT-29/19A cells assemble discontinuous AJs with oblique actin bundles that appear as intercellular stress fibers forming end-on attachments with the E-cadherin foci (Fig 4A, Top). Such discontinuous AJs have been seen in other cancer cells that have a hybrid E/M phenotype however, their role in tumorigenesis is unknown.(Ayollo et al., 2009; Gloushankova et al., 2017) In stark contrast, fascin1 KD cells formed continuous AJs with F-actin and E-cadherin distribution similar to normal epithelial cells. There was no discernable difference in the lateral junctions (Fig 4A, Middle). Overexpression of EGFP-Fascin1 in the *BRAF*<sup>V600E</sup> cell line HT-29 that lacks endogenous fascin1 confirmed fascin1's function in the remodeling of AJ associated actin cytoskeleton (Supplementary Figs 3A-3B). Moreover, this function of fascin1 was recapitulated in the non-transformed MDCK cells overexpressing EGFP-Fascin1 (Supplementary Fig 3C); and in the fascin1 KD shF cells overexpressing EGFP-Fascin1 (Supplementary Fig 3D) thereby demonstrating that this function of fascin1 is not cell type-specific.

*In vitro* fascin1 and  $\alpha$ -actinin mutually exclude each other to form discrete fascin1 or  $\alpha$ -actinin crosslinked actin networks.(Winkelman et al., 2016) We reasoned that in *BRAF*<sup>V600E</sup> CRC cells, fascin1 upregulation could result in a similar competitive exclusion of AJ associated actin bundling proteins like  $\alpha$ -actinin and potentially EPLIN. This would explain the AJ remodeling function of fascin1 in the *BRAF*<sup>V600E</sup> CRC cells. If true, such changes would also have significant implications for AJ mechanotransduction, because both  $\alpha$ -actinin and EPLIN regulate AJ mechanosensitivity.(Le et al., 2017; Taguchi et al.,

2011) Indeed in *BRAF*<sup>V600E</sup> Scr cells, fascin1 and  $\alpha$ -actinin segregate to different areas of the AJ-associated actin cytoskeleton (Fig 4B). While  $\alpha$ -actinin co-localized with the oblique actin bundles of the AJs, fascin1 was associated with the actin bundles where they attach to the E-cadherin foci (Fig 4B). This close proximity of fascin1 to the E-cadherin foci also suggests that in *BRAF*<sup>V600E</sup> CRC cells, fascin1 could play a direct role in regulating AJ mechanotransduction. As expected, we identified a competitive exclusion of  $\alpha$ -actinin and EPLIN away from the AJs to the cytoplasm of Scr cells (Figs 4C-4D). In shF cells, the  $\alpha$ -actinin and EPLIN distribution overlapped with the cell-cell margins, which is similar to their distribution in AJs of normal epithelial cell. Fascin1 also displaced  $\alpha$ -actinin away from focal adhesions (FAs) of Scr cells (Supplementary Fig 3E). However, there was no significant difference in total  $\alpha$ -actinin protein levels between control and fascin1 KD HT-29/19A cells (Supplementary Fig 3E). To quantitatively measure the effects of fascin1 on AJ actin dynamics, we transfected HT-29/19A-Scr and shF cells with mCherry-Lifeact (Fig 4E). As expected, kymographs revealed greater movement and greater velocity of movement of F-actin at the AJs of Scr cells compared to shF cells. To directly measure the effect of fascin1 KD on AJ mechanotransduction, we evaluated the association of vinculin with the AJs and the association of vinculin with  $\alpha$ -catenin. (Seddiki et al., 2018) In normal epithelial cells,  $\alpha$ -catenin is a key mechanosensor and monomeric  $\alpha$ -catenin ( $\alpha^M$ ) couples the E-cadherin- $\beta$ -catenin complex to the actin cytoskeleton and recruits vinculin to reinforce the AJ stability while the  $\alpha$ -catenin that dissociates from the cadherin-catenin complex homodimerizes ( $\alpha^D$ ). (Desai et al., 2013; Seddiki et al., 2018; Yao et al., 2014) In this manner  $\alpha$ -catenin and vinculin function as major mechanosensors that transmit the force of actomyosin

contractility to the E-cadherin- $\beta$ -catenin complex.(Fernandez-Sanchez *et al.*, 2015; Przybyla *et al.*, 2016; Yonemura *et al.*, 2010) While significant displacement of vinculin away from AJs (apical) and FAs (basal) to the cytoplasm was observed in HT-29/19A-Scr cells, fascin1 KD in HT-29/19A-shF cells restored vinculin localization to these cell adhesion sites which is similar to vinculin's distribution in normal epithelial cells (Fig 4F; Supplementary Fig 3E).(le Duc *et al.*, 2010) There was no significant difference in total vinculin protein levels between Scr and shF cells (Supplementary Fig 3E). Quantitative co-immunoprecipitation (IP) assay with an antibody that specifically immunoprecipitates monomeric  $\alpha$ -catenin revealed that fascin1 knockdown also resulted in higher levels of vinculin in complex with  $\alpha$ -catenin (Fig 4F).

***Fascin1 activates Wnt signaling in  $BRAF^{V600E}$  mutant CRC cells to drive primary and secondary tumor growth.*** We reasoned that by remodeling  $BRAF^{V600E}$  CRC cell AJ mechanotransduction, fascin1 could drive oncogenic Wnt activation. Indeed, subcellular fractionation showed that fascin1 KD significantly inhibited the nuclear accumulation of  $\beta$ -catenin (60.2%,  $n=3$ ,  $p<0.001$ ), and caused a redistribution of  $\beta$ -catenin from the nucleus and cytoplasm to the cell-cell margins and the AJs without impacting total  $\beta$ -catenin or E-cadherin protein levels (Fig 5A, Supplementary Figs 4A). Most notably, re-expression of EGFP-Fascin1 in the fascin1 KD shF cells resulted in the redistribution of  $\beta$ -catenin from the cell-cell margins and AJs back to the nucleus (Fig 5A) validating fascin1's direct role in nuclear accumulation of  $\beta$ -catenin. Actively invading Scr cell tumor spheroids confirmed significant nuclear accumulation of  $\beta$ -catenin (Fig 5B). Nuclear accumulation of  $\beta$ -catenin was also identified in MDCK cells overexpressing EGFP-Fascin1

(Supplementary Fig 4B). Likewise in the CRC patient cohort we identified tumors that were positive for both high fascin1 protein expression (score 2-3) and widespread (score 2) accumulation of nuclear  $\beta$ -catenin validating the pathophysiological significance of this function of fascin1 (Fig 5C).

Fascin1 KD in mutant *BRAF*<sup>V600E</sup> CRC cells also resulted in reduced expression of Wnt target genes including the marker for stemness, *CD44* and the ECM remodeling proteins, matrix metalloproteinases, *MMP7* and *MMP9* (Fig 5D). Reduced Wnt activation was confirmed by chromatin immunoprecipitation (ChIP-PCR) assay with the  $\beta$ -catenin antibody (Supplementary Fig 4C). Fascin1's function as a driver of Wnt activation was validated with the Super8x TOP-Flash luciferase TCF-LEF reporter assay (Supplementary Fig 4D). The reduction of Wnt activation induced by fascin1 KD was also accompanied by significant changes in epithelial cell behavior, including reduced anchorage-independent growth (Fig 5E), restoration of TJ morphology (Fig 5F), and contact inhibition-mediated growth inhibition (Fig 5F). Loss of contact inhibition was phenocopied in fascin1 KD shF cells overexpressing EGFP-Fascin1 cells (Supplementary Fig 5A) and in MDCK cells overexpressing EGFP-Fascin1 (Supplementary Fig 5B). Conversely, fascin1 KD in the *KRAS* mutant and wild type *BRAF* HCT-116 cells restored contact inhibition mediated growth inhibition validating this function of fascin1 is also not cell-type specific (Supplementary Figs 5C).

Next, we assessed the effects of fascin1 KD on primary and secondary tumor growth of *BRAF*<sup>V600E</sup> mutant CRC cells *in vivo*. Fascin1 KD significantly reduced primary tumor weight compared to control cells (Fig 6A;  $p < 0.01$ ,  $n = 6$ ) and reduced the number of actively proliferating tumor cells (Supplementary Fig 6A). More importantly, fascin1 KD induced a

re-localization of total and active (NP)  $\beta$ -catenin from the nucleus and cytoplasm to the cell membrane (Figs 6B-6C, respectively). We used the active (NP)  $\beta$ -catenin antibody to ascertain if the cytoplasmic  $\beta$ -catenin in these tumors is active. Most remarkably, in this *in vivo* model system, we validated the role of fascin1 in remodeling cell-cell junctions to assemble TM-like intercellular links (Fig 6D). Fascin1 KD also significantly reduced secondary tumor growth in mice (Fig 6E;  $p < 0.01$ ,  $n = 8$ ) and prevented the cytoplasmic and nuclear accumulation of total and active  $\beta$ -catenin (Fig 6E). Fascin1 KD also reduced CRC cell metastasis in a zebrafish embryo metastasis assay (Supplementary Fig 6B) validating this as a conserved function of fascin1.

***In CRCs fascin1 expression is linked to the E/M metastable state.*** Since fascin1 remodels AJ mechanotransduction, we postulated that fascin1 could also influence signals regulating epithelial-to-mesenchymal transition (EMT). Analysis of RNA-Seq data from CRCs profiled by the TCGA consortium, revealed a significant inverse correlation between mRNA expression of fascin1 and the epithelial phenotype stability factors (PSFs) *OVOL1* and *GRHL2* (Fig 7A) and conversely, a significant positive correlation with the metastable markers *SNAI1/2/3*. (Jolly et al., 2016) The modest inverse correlation of fascin1 with *OVOL* and *GRHL2* suggests dampening of epithelial characteristics but not complete EMT and the positive correlation with *SNAI* suggests stabilization of the E/M state. We also identified a significant positive correlation between fascin1 and *ZEB1/2* expression. Since stromal cells (e.g. fibroblasts) also express fascin1 and *ZEB1/2* proteins, we also performed these analyses in RNA-Seq data obtained from 61 CRC cell lines, which revealed similar findings confirming these changes were tumor intrinsic (Fig

7B). Previously, it has been reported that in a mutant *Apc* model of CRC, fascin1 is upregulated in intestinal tumors which is consistent with induction of fascin1 expression in CRCs.(Hashimoto *et al.*, 2006; Schoumacher *et al.*, 2014) Based on that we elected also to examine the expression of these TFs in the normal mucosa and intestinal tumors derived from mutant *Apc* mice. These studies revealed a significant upregulation of fascin1 and *Snai3* mRNA in intestinal tumors but no change in the levels of *Ovol1*, *Grhl2* or *Zeb1/2* (Supplementary Fig 6C).

***Fascin1 promotes collective cell migration.*** As collective cell migration is a hallmark of the hybrid E/M metastable state, we assessed the role of fascin1 in a wound-closure assay. As expected, fascin1 overexpression significantly increased cell migration rates in MDCK cells (Supplementary Videos 3-4; Fig 7C). We identified three groups of migrating EGFP-Fascin1 cells that we refer to as loose, edge and bulk, which migrated at different speeds and with different patterns (Supplementary Video 3-4; Supplementary Table 1; Figs 7D-7E). Loose and edge cells migrated using TM-like structures connecting the back of a leading cell with the front of a follower cell (Supplementary Videos 3-4, Supplementary Fig 7A). By measuring the area of migrating bulk cells, it is clear that migrating bulk cells also remodel cell-cell adhesions (Supplementary Videos 3 and 4; Supplementary Fig 7B). Moreover, while control MDCK cells migrated as a sheet of tightly adherent cells, fascin1 overexpressing MDCK cells displayed large gaps within the migrating cell clusters, indicative of increased tension at cell-cell adhesion sites and continuous AJ remodeling during cell migration (Supplementary Videos 3 and 4; Supplementary Fig 7D). Additionally, we made the striking finding that fascin1

overexpressing loose cells display significantly more backwards migration events in the direction opposite from the wound edge, which were quantitatively measured by the shape metrics (Supplementary Video 4; Figs 7D-7E, Supplementary Fig 7C, Supplementary Table 2). Based on the analysis of X and XY (radial) coordinates, the backwards migration of EGFP-Fascin1 cells was significantly different from the consistent forward migration of MDCK-EGFP cells. Villin1 is an actin bundling protein that assembles filopodia and increases intestinal cell migration rates in normal intestinal epithelium.(George et al., 2013) However, MDCK cells overexpressing EGFP-Villin1 migrated unidirectionally as a sheet of tightly adherent cells underscoring this unique behavior of fascin1 overexpressing cells (Supplementary Video 5).

## Discussion

Even though fascin1 has been identified as a driver and prognostic marker of metastatic CRCs a systematic characterization of fascin1 function in the etiology of CRCs is lacking.(Ristic *et al.*, 2021) Fascin1 expression is very significantly upregulated in SSLs and fascin1 has been identified as a potential biomarker of SSLs.(Ashktorab *et al.*, 2019; Kanth *et al.*, 2019; Kanth *et al.*, 2016). A careful evaluation of multi-omic data presented in a recent study by Chen *et al* revealed that fascin1 mRNA is significantly upregulated in serrated but not conventional colorectal polyps.(Chen *et al.*, 2021) Almost a decade ago, Conesa-Zamora *et al* reported that fascin1 was one of two genes that was differentially expressed in serrated adenocarcinomas compared to conventional carcinomas.(Conesa-Zamora *et al.*, 2013) More notably, the authors reported a worse prognosis for fascin1 expressing serrated adenocarcinomas which is in agreement with other reports of fascin1

upregulation in CRCs.(Conesa-Zamora *et al.*, 2013; Hashimoto *et al.*, 2006) Despite this strong association of fascin1 with serrated pathway carcinogenesis, the functional characterization of fascin1 in the progression of serrated pathway carcinomas has not been directly investigated. Conesa-Zamora *et al* also reported that fascin1 upregulation was statistically associated with KRAS mutation.(Conesa-Zamora *et al.*, 2013) Our results are in agreement with those of Conesa-Zamora *et al* that fascin1 is upregulated in serrated carcinomas additionally, we show that fascin1 expression is statistically associated with BRAF<sup>V600E</sup> mutation. Previously, BRAF<sup>V600E</sup> mutation was shown to drive dedifferentiation and our study shows that indeed fascin1 upregulation in CRCs positively correlates with tumor dedifferentiation.(Herr *et al.*, 2015; Reischmann *et al.*, 2020) While the underlying genes that drive serrated pathway carcinogenesis and the molecular changes that are required for metastatic progression of SSLs remain poorly defined, upregulation of genes involved in matrix remodeling, cell migration/invasion and EMT are all implicated.(De Sousa *et al.*, 2013) Here we identify, for the first time, a direct role for fascin1 in Wnt activation and an upregulation of Wnt target genes associated with ECM remodeling such as *MMP-7* and *MMP-9*.(Lin *et al.*, 2021) Additionally, our studies identify fascin1's function in BRAF<sup>V600E</sup> CRC cell migration and invasion as well as the association of fascin1 with hybrid EMT. These canonical and non-canonical functions of function1 in underscore the pivotal role of fascin1 in serrated pathway carcinogenesis. Little is known about the molecular events driving the initiation and progression of BRAF<sup>V600E</sup>-mutant CRCs although BRAF<sup>V600E</sup> mutation is linked to AJ and TJ remodeling.(Conesa-Zamora *et al.*, 2013; Herr *et al.*, 2015) Here we show that in BRAF<sup>V600E</sup> CRC cells, AJ and TJ remodeling is phenocopied by fascin1 upregulation and we identify fascin1 as a major

driver of this *BRAF*<sup>V600E</sup>-mutant CRC phenotype.(Herr *et al.*, 2015) Fascin1's upregulation in SSLs and in serrated/*BRAF*<sup>V600E</sup> CRCs together with its direct role in Wnt activation suggests that in the serrated pathway, fascin1 could regulate both tumor initiation and progression. Our hypothesis is supported by a previous report where constitutive expression of fascin1 in the intestinal epithelium in the *Apc*-mutated mouse background was shown to significantly decrease survival and increase tumor burden providing evidence that fascin1 regulates intestinal tumor initiation.(Schoumacher *et al.*, 2014)

In this study, we demonstrate for the first time a direct role for fascin1 in the assembly of remodeled cell-cell junctions that resemble TMs. We show that these TM-like structures contain E-cadherin and  $\beta$ -catenin, which suggests that the origins of these structures is similar to epithelial protrusions that assemble and/or repair AJs.(Li *et al.*, 2020) These findings also indicate that when upregulated in *BRAF*<sup>V600E</sup> CRC cells fascin1 appropriates this molecular machinery to construct TM-like remodeled cell-cell junctions. We show that in *BRAF*<sup>V600E</sup> CRC cells these TM-like structures share many structural and functional similarities with protrusions associated with TNTs, neuronal growth cones and TMs such as their morphology, their inclusion of tubulin and organelles, and their ability to hover over cell surfaces while connecting distant cells.(Osswald *et al.*, 2015; Rustom *et al.*, 2004) The most significant difference that makes these remodeled cell-cell junctions more TM-like is their longer lifespan as seen in MDCK EGFP-Fascin1 cells (>60 min) and in primary tumors in mice. Unlike its distribution in migrating cells and more like its distribution in growth cones, fascin1 localizes to the lamellipodia- and filopodia-like protrusions of the remodeled cell-cell junctions.(Cohan *et al.*, 2001) TNTs are thought to

correspond to invadopodia *in vivo* and TMs *in vivo* have been shown to regulate tumor cell migration/invasion but also tumor proliferation and radioresistance.(Naphade et al., 2015; Osswald *et al.*, 2015) While these TM-like structures remain to be identified in serrated pathway CRCs, we hypothesize that this property of fascin1 implicates it in *BRAF*<sup>V600E</sup> CRC invasion, proliferation and chemoresistance and underscores fascin1's impact on the pathogenesis of the serrated pathway cancers. We speculate that these TM-like structures could also have other functions e.g. as conduits for cell signaling allowing cells at the invasive front and the tumor center to communicate directly, or to function like cytonemes to traffic morphogens and to generate morphogen gradients. Since stromal cells also expression fascin1, morphogen trafficking between the stromal and tumor cells can be envisioned. We speculate that such properties of remodeled TM-like cell-cell junctions could influence CRC tumor heterogeneity. Tumor heterogeneity is responsible for the failure of most cancer therapies and this may be the molecular basis for fascin1's association with treatment-refractory CRCs.

Our study shows that in *BRAF*<sup>V600E</sup> CRC cells, fascin1 regulates the competitive exclusion of three major AJ associated mechanosensors namely,  $\alpha$ -actinin, EPLIN, and vinculin. Fascin1 and  $\alpha$ -actinin form actin bundles with very different inter-filament spacing, 8 nm *versus* 35 nm, respectively.(Winkelman *et al.*, 2016) We propose that in *BRAF*<sup>V600E</sup> CRC cells, the tightly packed actin bundles formed by fascin1 exclude non-muscle myosin II (NMII) and this could be the molecular basis for the segregation of the two proteins in the AJ associated actin cytoskeleton. Both fascin1 and  $\alpha$ -actinin assemble stable actin networks but when these structures are mixed together they form unstable structures because  $\alpha$ -actinin crosslinks impose unfavorable and energetically costly defects in

hexagonally packed structures formed by fascin1 and *vice versa*.(Freedman et al., 2019)

We propose that such energetically costly defects in fascin1 expressing *BRAF*<sup>V600E</sup> CRC cells likely remodel AJ actin dynamics and increase AJ plasticity. More importantly, we demonstrate unequivocally that in *BRAF*<sup>V600E</sup> CRC cells fascin1 KD restores AJ morphology and function comparable to normal epithelial cells. In the quiescent epithelium, mechanical strain is sufficient to activate  $\beta$ -catenin and cell cycle re-entry.(Benham-Pyle *et al.*, 2015; Fernandez-Sanchez *et al.*, 2015; Roper et al., 2018) We propose that the profound changes in AJ actin cytoskeleton and AJ mechanotransduction regulated by fascin1 are sufficient for aberrant Wnt activation in the serrated pathway. Despite a high prevalence in CRCs, ectopic expression of an oncogenic *BRAF*<sup>V600E</sup> mutant transgene in mice promotes senescence or differentiation of intestinal stem cells.(Riemer et al., 2015; Tong *et al.*, 2017) However, elevated Wnt signaling can rescue the stem cell loss in *BRAF*<sup>V600E</sup> mutant mice to drive serrated pathway carcinogenesis.(Reischmann *et al.*, 2020; Riemer *et al.*, 2015; Tong *et al.*, 2017) We hypothesize that this may be the molecular significance of aberrant Wnt signaling in SSLs and in serrated pathway CRCs. Based on that we propose that fascin1 upregulation in SSLs and serrated pathway CRCs contributes to oncogenic transformation after *BRAF*<sup>V600E</sup> activation by directly activating Wnt signaling. We propose that such coordination of aberrant Wnt signaling by fascin1 with *BRAF*<sup>V600E</sup> activation regulates CRC initiation and progression. Mechanical cues can initiate tumor-like gene expression pattern in pre-neoplastic tissues of the *Apc* mutant mice.(Whitehead *et al.*, 2008) This suggests that in patients with mutant *APC*, colon epithelial cells are hypersensitive to mechanical perturbations. A similar function for mutant *APC* could also explain why the

conditional expression of fascin1 in mutant *Apc* mice promotes both tumor initiation and progression.(Schoumacher *et al.*, 2014) It may be noted that even in the absence of conditional fascin1 expression in the mutant *Apc* mice, endogenous fascin1 expression in this mouse model of CRC has been reported previously and is validated by us here (Supplementary Fig 6C).(Schoumacher *et al.*, 2014) In intestinal organoids BRAF<sup>V600E</sup> mutation induces transient proliferation, inhibits epithelial organization but eventually leads to the disintegration of the organoid.(Reischmann *et al.*, 2020) However, *Apc* deletion in these organoids prevents their disintegration and confers growth factor independence suggesting a cooperation between BRAF<sup>V600E</sup> and mutant *Apc* signaling.(Reischmann *et al.*, 2020) In the study of Conesa-Zamora *et al* fascin1 expression was observed in 88.6% of serrated adenocarcinomas but also in 14.3% of conventional carcinomas.(Conesa-Zamora *et al.*, 2013) Our study shows that one-third of all CRCs express fascin1, which allows us to speculate that even in the presence of mutant APC, fascin1 may be the driver of aggressive, metastatic CRCs and an important regulator of oncogenic Wnt signaling. One previous study has shown that in CRC cells fascin1 is itself a target of  $\beta$ -catenin-TCF signaling.(Vignjevic *et al.*, 2007) While we did not see a similar effect of Wnt signaling on fascin1 expression, a feedback mechanism between Wnt and fascin1 is possible. Targeted Wnt therapies for the treatment of CRCs have been unsuccessful due to the pleiotropic effects of Wnt. Most of these drugs also target ligand-receptor Wnt signaling, a likely factor in their ineffectiveness. The fascin1 knockout mice do not have any major defects, and since fascin1 is absent from the normal colon, we propose that fascin1 is a potential therapeutic target to prevent aberrant Wnt activation in serrated/*BRAF*<sup>V600E</sup> CRCs.

The expression of TFs such as *OVOL* and *ZEB* and *OVOL* and *SNAI* induce the hybrid E/M metastable state.(Jia et al., 2017) Our study reveals that fascin1 expression in CRCs is linked to the hybrid E/M state. Even in the mutant *Apc* mouse model, we found fascin1 upregulation associated with a hybrid E/M phenotype. While we predict that the majority of carcinomas expressing fascin1 will have an E/M phenotype, some fascin1 expressing cancers could reflect a complete phenotypic transition to M due to rewiring of EMT regulatory networks and/or differences in epigenetic reprogramming. Fascin1 expressing CRC cells migrate collectively using TM-like remodeled cell-cell connections which could function *in vivo* as guidance cues. This is supported by the knowledge that similar AJ elongation during morphogenesis provides directional cues.(Niewiadomska et al., 1999) We also interpret this as reactivation of embryonic cell migration patterns in *BRAF<sup>V600E</sup>*-mutated CRCs. We predict that TM-like structures provide *BRAF<sup>V600E</sup>* CRCs with an advantage when responding to external cues by rapidly remodeling AJs allowing CRC cells to switch between more closely or more loosely adherent cells leading to successful metastasis. Bidirectional migration of leukocyte T cells and vertebrate axon growth cones is regulated by chemoattraction and chemorepulsion.(Poznansky et al., 2000; Vianello et al., 2005) We propose that by facilitating bi-directional migration fascin1 could enhance the response of *BRAF<sup>V600E</sup>* CRCs to chemoattractants and chemorepellents to promote successful tumor metastasis. It is clear that other actin crosslinking proteins like villin1, which are also expressed in most CRC cells, cannot fulfill this function. This may also explain why fascin1 is upregulated in metastatic CRCs. In summary, we provide for the first time, a functional characterization of fascin1 in serrated neoplasia pathway and identify fascin1's novel role in this pathway that contributes to tumor growth and

metastasis. Our study provides a molecular mechanism for aberrant Wnt activation that has previously been shown to drive serrated pathway carcinogenesis. We postulate that targeting fascin1's function in AJ remodeling could provide a novel, effective therapeutic approach to prevent aggressive, recurrent, treatment refractory, serrated pathway CRCs, which could lead to improved patient survival.

**Acknowledgement:** This study was supported by National Institutes of Diabetes and Digestive Kidney Diseases (grant DK-117476 to S.K.); and the Public Health Service (grant DK-56338).

**Author Contributions:** Eric Pham, Amin Esmaeilniakooshkghazi, Sudeep P. George, Afzal Ahrorov, Fabian R. Villagomez, Michael Byington, Srijita Mukhopadhyay, Srinivas Patnaik, Monali Naik and Saathviaka Ravi, Niall Tebuttt, Jennifer Mooi, Camilla M. Reehorst performed the experiments described in this study. Jacinta C. Conrad analyzed the migration data and provided important guidance for the experimental design of these studies. John M. Mariadason is a long-standing collaborator of the contributing author and provided the patient cohort data, analyzed the patient cohort data as well as provided valuable suggestions during the writing of this manuscript.

**Conflict of Interest:** The authors declare no potential conflict of interest exists.

## Figure Legends

**Figure 1. The role of fascin1 in serrated/*BRAF*<sup>V600E</sup> CRCs.** (A-B) CRCs were graded for fascin1 protein expression and Venn diagram and pie chart show the correlation of fascin1 with CRCs and with *BRAF*<sup>V600E</sup>-mutant CRCs. (C) Phase contrast image of HT-29/19A-Scr and shF cells grown as suspension 48 h tumor spheroids. Scale bar, 25 µm. (D) Confocal images of sub confluent HT-29/19A-Scr and HT-29/19A-shF cells show distribution of actin (red) and tubulin. Nuclei were counter stained with DAPI. Scale bar, 50 µm (Scr) and 10 µm (shF). (E) Confocal image of sub confluent HT-29/19A-Scr cells shows distribution of actin (magenta), tubulin (red), and fascin1 (green). Nuclei were counter stained with DAPI. Scale bar, 30 µm. (F) Confocal image of HT-29/19A-Scr cells shows distribution of actin (red), tubulin (cyan) and E-cadherin (green). Nuclei were counter stained with DAPI. Scale, 10 µm.

**Figure 2. Fascin1 remodels AJ assembly in *BRAF*<sup>V600E</sup> CRC cells.** (A) Confocal image of Scr and shF cells shows distribution of actin (green), E-cadherin (red) and β-catenin (cyan) as two cells (cell 1 and 2) assemble nAJs. Arrowheads identify, oblique actin bundles, E-cadherin and β-catenin foci (white). Elongated nascent cell-cell junctions with or without distal lamellipodia (cyan). bottom panel is a magnification of the boxed area. Scale, 20 µm. (B) Confocal image of MDCK EGFP-Fascin1 cells shows distribution of fascin1 (green) and E-cadherin (red). Scale bar, 20 µm. (C) Confocal image of MDCK EGFP-Fascin1 cells shows the distribution of fascin1 (green) and β-catenin (red) during nAJ assembly. Bottom panels are magnification of the boxed areas shown above. Scale bar, 10 µm. (D) Confocal image MDCK EGFP-Fascin1 cells shows growth-cone like

cellular protrusion during nAJ assembly. Scale bar, 20  $\mu\text{m}$ . **(E)** Live confocal immunofluorescence of MDCK EGFP-Fascin1 cells labeled with MitoTracker-Red and LysoTracker Red show the presence of functional mitochondria and lysosomes in these elongated nascent AJs. Asterisks highlight mitochondria and lysosomes, respectively. Scale bar, 10  $\mu\text{m}$ .

**Figure 3: Fascin1 assembles tumor microtube-like elongated cell-cell junctions. (A)**

Confocal immunofluorescence z-stacks (xy images; 1  $\mu\text{m}$  each from (a) to (f)) show the distribution of fascin1 (green) and actin (red) in confluent MDCK EGFP-Fascin1 cells. Arrowhead identifies TM-like intercellular junctions connecting cell 1 to cell 6. Scale bar, 15  $\mu\text{m}$ . **(B)** Live confocal immunofluorescence z stacks (xy images; 1  $\mu\text{m}$ ) of MDCK EGFP-Fascin1 cells show TM-like cell-cell junction suspended over the confluent monolayer. Scale bar, 25  $\mu\text{m}$ . **(C)** Phase contrast images show clusters of MDCK EGFP and MDCK EGFP-Fascin1 cells at time 0 and at 17.5 h post-treatment with HGF. Scale bar, 20  $\mu\text{m}$ . **(D)** Correlation of TM-like remodeled cell-cell junction length ( $\mu\text{m}$ ) and lifespan (hrs) in HGF treated MDCK EGFP and MDCK EGFP-Fascin1.

**Figure 4. Fascin1 remodels AJ associated actin cytoskeleton in *BRAF*<sup>V600E</sup> CRC cells. (A)**

Confocal microscopy shows the distribution of actin (red) and E-cadherin (green) at the AJs (Top) and lateral junctions (Middle) of HT-29/19A-Scr and shF cells. Nuclei were counter stained with DAPI. Plot profiles were generated by measuring the distribution of actin and E-cadherin in ROI highlighted by a white line, 10  $\mu\text{m}$  long. Scale, 10  $\mu\text{m}$ . **(B)** Virtual Channel confocal microscopy shows the AJ associated actin (red),

fascin1 (green) and  $\alpha$ -actinin (cyan) in Scr cells. Scale bar, 10  $\mu$ m. **(C)** Confocal immunofluorescence of HT-29/19A-Scr and shF cells show the distribution of E-cadherin (green) and  $\alpha$ -actinin (red) at the AJs. Nuclei were counter stained with DAPI. Plot profiles were generated by measuring the distribution of E-cadherin and  $\alpha$ -actinin in ROI highlighted by a white line, 10  $\mu$ m long. Scale bar, 10  $\mu$ m. **(D)** Virtual Channel confocal immunofluorescence of HT-29/19A-Scr and shF cells shows distribution of actin (red), E-cadherin (cyan), and EPLIN (green) at the AJs. Nuclei were counter stained with DAPI. Plot profiles were generated by measuring the distribution of EPLIN and actin in ROI highlighted by a white line, 10  $\mu$ m long. Scale bar, 10  $\mu$ m. **(E)** Live cell imaging of HT-29/19A-Scr and shF cells stably expressing mCherry-Lifeact. Nuclei were counter stained with Hoechst. Scale bar, 5 $\mu$ m. Kymograph analysis of mCherry-Lifeact at AJs of Scr and shF cells measured at two ROI (labeled 1 and 2, 10  $\mu$ m each) shows difference in speed ( $\mu$ m/min) of migration and distance ( $\mu$ m/min) moved by AJ-associated F-actin in Scr and shF cells. Asterisk (\*\*\*\*) denotes  $p < 0.001$ ,  $n = 6$ . **(F)** Confocal images of Scr and shF cells show xz distribution of vinculin (green) and actin (red). Nuclei were counter stained with DAPI. Scale bar, 10  $\mu$ m. Accumulation of cytoplasmic vinculin in Scr and shF cells was measured from three independent experiments (\*\*\*) denotes  $p < 0.001$ ,  $n = 3$ . Scr and shF cell lysates were immunoprecipitated with  $\alpha$ -catenin antibody and immunoblotted with vinculin antibodies. Asterisks (\*) denote as follows: \*\*\* denotes  $p < 0.001$ ,  $n = 3$  and \*\*\*\*  $p < 0.0001$ ,  $n = 3$ .

**Figure 5. Fascin1 activates Wnt signaling.** **(A)** Confocal immunofluorescence of HT-29/19A-Scr, shF and shF expressing Fascin1 shows the distribution of total  $\beta$ -catenin

(green). Nuclei were counter stained with DAPI. Scale bar, 10  $\mu$ m. Subcellular fractionation assays were performed to quantify the distribution of  $\beta$ -catenin in the nuclear (N), cytoplasmic (C) and whole cell (WC) lysate fractions. Asterisk (\*\*\*\*) denotes  $p < 0.0001$ ,  $n = 3$ . **(B)** Phase contrast image shows actively invading Scr cell tumor spheroids at day 0 and at the end of day 8. Confocal images show the distribution of fascin1 (green) and  $\beta$ -catenin (red) in actively invading Scr cell tumor spheroids. Nuclei were counter stained with DAPI. Right panels (i) and (ii) are magnifications of the boxed areas labelled (i) and (ii). **(C)** Immunohistochemistry in paired panels show fascin1 and widespread nuclear  $\beta$ -catenin accumulation in the same colorectal tumor. Arrowheads highlight widespread accumulation of nuclear  $\beta$ -catenin in high fascin1 expressing tumors. **(D)** Quantitative RT-PCR for Wnt target genes using total cellular mRNA extracted from Scr and shF cells. Asterisks (\*) denote as follows: \*  $p < 0.05$ , \*\*  $p < 0.01$ , \*\*\*  $p < 0.001$  ( $n = 6$ ). **(E)** Phase contrast image of anchorage-independent colonies of HT-29/19A-Scr and shF cells. Asterisk (\*) denotes  $p < 0.05$ ,  $n = 3$ . **(F)** Confocal immunofluorescence shows xz distribution of ZO-1 (green) and actin (red) (left panels) and xz distribution of actin (red) and Ki67 (green; right panels) in Scr and shF cells. Nuclei were counter stained with DAPI. Asterisk (\*\*\*) denotes  $p < 0.001$ ,  $n = 3$ .

**Figure 6. Fascin1 activates Wnt signaling in *BRAF*<sup>V600E</sup> mutant CRC cells to drive primary and secondary tumor growth in mice.** **(A)** IVIS imaging of NSG mice injected subcutaneously with *BRAF*<sup>V600E</sup> mutant HT-29/19A-Scr and shF cells. Fascin1 KD significantly decreased primary tumor weight. Asterisk (\*\*) denotes  $p < 0.001$ ,  $n = 6$ . **(B)** Confocal immunofluorescence shows distribution of total  $\beta$ -catenin in primary tumors of

mice injected with Scr and shF cells. Nuclei were counter stained with DAPI. Scale bar, 10  $\mu$ m. **(C)** Immunohistochemistry shows distribution of active (NP)  $\beta$ -catenin in primary tumors from mice injected with *BRAF*<sup>V600E</sup> mutant HT-29/19A-Scr or shF cells. Yellow arrowheads label nuclear accumulation of active  $\beta$ -catenin. **(D)** Confocal image of primary tumor from Scr injected mice shows TM like remodeled AJs and the distribution of actin (red) and fascin1 (green) in these remodeled cell-cell junctions (arrowhead). Nuclei were counter stained with DAPI. Right panel is a magnification of the boxed area. **(E)** Secondary tumor growth in liver of mice injected with Scr or shF cells. Asterisk (\*\*) denotes  $p < 0.0001$ ,  $n = 8$ . Immunohistochemistry of secondary tumors from mice injected with Scr and shF cells shows distribution of fascin1, total  $\beta$ -catenin and active (NP)  $\beta$ -catenin in tumor (T) and surrounding normal (N) tissue. White arrowheads identify nuclear accumulation of  $\beta$ -catenin.

**Figure 7. Upregulation of fascin1 expression correlates with a hybrid E/M metastable state.** **(A-B)** Correlation analysis of mRNA expression levels of fascin1 with epithelial (*OVOL1*, *OVOL2* and *GRHL2*), mesenchymal (*ZEB1* and *ZEB2*), and E/M stability markers (*SNAIL1*, *SNAIL2*, *SNAIL3*) in **(A)** CRCs,  $n = 273$ , and **(B)** CRC cell lines,  $n = 61$ . **(C)** Phase contrast image of scratch wound of MDCK control cells expressing EGFP or overexpressing EGFP-Fascin1. Cells identified by our tracking method are shown in green (bulk), red (edge) or blue (loose). Scale bar, 50  $\mu$ m. See methods for description of group classifications. Quantification of instantaneous migration speeds are shown as mean ( $\bar{x}$ )  $\pm$  SD. P-value from Mann-Whitney U test comparing MDCK EGFP and MDCK EGFP-Fascin1 cells. **(D)** Quantification of instantaneous migration velocity in

X coordinates only and in XY-radial coordinates. Instantaneous migration velocity frequencies in XY-radial coordinates. **(E)** Instantaneous velocity-angle histograms of migrating MDCK EGFP and MDCK EGFP-Fascin1 bulk, edge, and loose cell clusters.

**Supplementary Figure 1. (A)** Fascin1 expression increases significantly with increasing tumor grade (G1>G2>G3, \*\* $p<0.01$ ,  $n=270$ ).

**Supplementary Figure 2. (A)** Endogenous fascin1 expression in HT-29/19A-Scr and HT-29/19A-shF cells and ectopic overexpression of EGFP-Fascin1 in HT-29/19A-shF cells. Tubulin was used as a loading control. This immunoblot is a representative of at least three independent experiments with similar findings. **(B)** Confocal immunofluorescence shows distribution of F-actin (red), tubulin (green) and fascin1 (magenta) in nAJs of Scr cells. Nuclei were counter stained with DAPI. Scale bar, 30  $\mu\text{m}$ . **(C)** Phase contrast image of HT-29/19A-Scr and shF cells. Scale bar, 10  $\mu\text{m}$ . Rate of elongated nAJ assembly was measured in HT-29/19A-Scr and shF cells. Data are presented as mean  $\pm$  S.E.M.; Students's t-test. Asterisk (\*\*\*) denotes  $p<0.001$ ,  $n=10$  fields/group and  $>300$  cells/group. **(D)** Phase contrast image of HT-29/19A-Scr cells. Scale bar, 10  $\mu\text{m}$ . Rate of elongated nAJ assembly was measured in Scr cells 48 h post-treatment with vehicle control (DMSO), cytochalasin B (250 nM), or colchicine (1 mM). Data are presented as mean  $\pm$  S.E.M.; Students's t-test. Asterisk (\*\*\*) denotes  $p<0.001$ ,  $n=10$  fields/group and  $>300$  cells/group. Asterisk (\*\*\*\*) denotes  $p<0.0001$ ,  $n=10$  fields/group and  $>300$  cells/group. **(E)** Ectopic overexpression of EGFP-Fascin1 in MDCK cells. Tubulin was used as a loading control.

**Supplementary Figure 3. (A)** Immunoblot shows ectopic overexpression of EGFP and EGFP-fascin1 in HT-29 cells, a *BRAF*<sup>V600E</sup> CRC cell line that lacks endogenous fascin1 protein. Tubulin was used as a loading control. This immunoblot is a representative of at least three independent experiments with similar findings. **(B)** Confocal immunofluorescence of HT-29 EGFP and HT-29 EGFP-Fascin1 cells shows distribution of AJ associated actin (red) and EGFP (green). Nuclei were counter stained with DAPI. Scale bar, 10  $\mu$ m. **(C)** Confocal image of MDCK EGFP and MDCK EGFP-Fascin1 cells shows distribution of AJ associated actin (red) and EGFP (green). Nuclei were counter stained with DAPI. Scale bar, 10  $\mu$ m. **(D)** Confocal image of shF cells overexpressing EGFP or EGFP-Fascin1 shows distribution of AJ associated actin (red) and EGFP (green). Scale bar, 10  $\mu$ m. **(E)** Confocal image shows the distribution of focal adhesion associated actin (red),  $\alpha$ -actinin (green) and vinculin (green) in Scr and shF cells. Right panels are magnifications of the boxed areas. Immunoblot shows total vinculin, fascin1 and  $\alpha$ -actinin levels in Scr and shF cells. Tubulin was used as a loading control. This immunoblot is a representative of at least three independent experiments with similar findings.

**Supplementary Figure 4. (A)** Immunoblot shows total E-cadherin and  $\beta$ -catenin levels in Scr and shF cells. Tubulin was used as a loading control. This immunoblot is a representative of at least three independent experiments with similar findings. **(B)** Confocal immunofluorescence z-stack of MDCK EGFP-Fascin1 cells shows distribution of fascin1 and  $\beta$ -catenin. Nuclei were counter stained with DAPI. Scale bar, 20  $\mu$ m. Data

obtained from  $n = 10$  fields/group, and  $>15$  cells/group. **(C)** ChIP-qPCR with  $\beta$ -catenin antibody and cell lysates from HT-29/19A-Scr and shF cells. ChIP with IgG and negative control primers against a region of MMP9 were used as control. Data are representative of  $n=3$  biological replicates, mean  $\pm$  S.E.M.; Student's t-test. Asterisk (\*) denotes  $*p<0.05$ ,  $n=3$ . NS, not significant, **(D)** Wnt signaling activity in *BRAF*<sup>V600E</sup> mutant HT-29/19A-Scr and shF cells was monitored using TOPFlash luciferase reporter assay. Data are shown as mean  $\pm$  S.E.M., Student's t-test. Asterisk (\*) denotes  $p<0.01$ ,  $n=3$ .

**Supplementary Figure 5. (A)** Confocal image of shF EGFP and shF EGFP-Fascin1 cells shows xz distribution of actin (red) and EGFP (green). Nuclei were counter stained with DAPI. Scale bar, 10  $\mu$ m. **(B)** Confocal image of MDCK EGFP and MDCK EGFP-Fascin1 cells shows xz distribution of actin (red) and EGFP (green). Nuclei were counter stained with DAPI. Scale bar, 10  $\mu$ m. **(C)** Confocal image shows xz distribution of actin (red) in HCT-116 expressing scrambled shRNAs (Scr) and HCT-116 cells transduced with shRNAs to KD fascin1 (shF cells). Nuclei were counter stained with DAPI. Scale bar, 10  $\mu$ m. Immunoblot shows total fascin1 levels in HCT-116 cells expressing scrambled shRNA (Scr) and HCT-116 with fascin1 KD using fascin1 specific shRNA (shF). Actin was used as a loading control. This immunoblot is a representative of at least three independent experiments with similar findings.

**Supplementary figure 6. (A)** Confocal immunofluorescence of primary tumors from mice injected with Scr or shF cells labeled for cell proliferation (Ki67, green) and apoptosis (cleaved caspase-3, red). Nuclei were counter stained with DAPI. Scale bar, 10  $\mu$ m. **(B)**

Scr and shF cells labeled with dye (red) injected into 2-day old zebrafish embryos and metastasis scored for 72 h post-injection. This is a representative of three independent experiments with similar findings. **(C)** Analysis of mRNA expression levels of fascin1; (*OVOL1* and *GRHL2*), mesenchymal (*ZEB1* and *ZEB2*), and E/M stability markers (*SNAIL1*, *SNAIL2*, *SNAIL3*) in intestinal tumors and normal intestinal tissue from mutant *Apc* mice. Asterisks denote the following: \*\* $p < 0.001$ ,  $n = 5$  and \*\*\*\* $p < 0.0001$ ,  $n = 5$ .

**Supplementary figure 7 (A)** Phase contrast microscopy shows TM-like long intercellular junction connecting two migrating MDCK EGFP-Fascin1 loose cells. Arrowheads indicates the TM-like structure. **(B)** Total area ( $\mu\text{m}^2$ ) covered by 'bulk' cells was measured in migrating MDCK EGFP and MDCK EGFP-Fascin1 cells. Asterisk (\*\*\*\*) denotes  $p < 0.0001$ ,  $n = 3$ . **(C)** Time lapse phase contrast imaging of MDCK EGFP-Fascin1 cells captured every 10 min. Start time, 20:30 and finish time, 1:02:40 **(D)** Large gaps (arrowheads) identified in migrating MDCK EGFP-Fascin1 cells.

## Methods

**Cells and plasmids:** HT-29/19A, HCT-116 and MDCK cells are described by us previously.(Mathew et al., 2008; Patnaik et al., 2016) MRC-5, HT-29 cells were purchased from American Type Culture Collection (ATCC, Rockville, MD). Human fascin1 plasmid was a kind gift from Dr. Shigeko Yamashiro (Rutgers University, New Brunswick, NJ). HT-29/19A and HCT-116 cells were transduced with lentivirus expressing short-hairpin RNAs (shRNAs) targeting fascin1 (Sigma-Aldrich, St. Louis, MO). For the rescue experiments, EGFP-Fascin1 plasmid without 3'UTR region were overexpressed in HT-29/19A-shF cells. EGFP-Fascin1 or EGFP were also overexpressed in HT-29 cells that lack endogenous fascin1 protein.

**Tumor spheroid culture:** Tumor spheroids were generated as described previously.(Humtsoe et al., 2012) Briefly, cells were grown on standard tissue culture dishes to 80% confluence, and re-plated 24 h prior to initiating tumor spheroids. For tumor spheroids  $1 \times 10^6$  cells/mL were plated on agarose-coated dishes. Spheroids were imaged using a Nikon Eclipse TE2000-U inverted microscope equipped with a CoolSnap ES charge-coupled device (CCD) camera. For hanging drop cultures, 2000 cells in 20  $\mu$ l drops were plated on the inside lids of 10 cm dishes, and the lids were inverted prior to incubation.

**Immunoblotting:** Cell lysates were prepared as described previously.(Wang et al., 2016) Briefly, proteins were separated by SDS-PAGE, transferred to nitrocellulose membranes,

immunoblotted and detected with ECL. All Western blots are representative of at least three independent experiments with similar findings.

**Cell migration assay:** Migration assay was performed as described previously.(George *et al.*, 2013) Briefly, cells were plated on 6-well tissue culture treated dishes and allowed to grow to confluency. Upon confluency, the monolayers were wounded with a sterile blade. Wells were rinsed with phosphate buffered solution (PBS), and cells were treated with MRC-5 conditioned media (diluted in 3 volumes 10% FBS DMEM). Cells were treated for 20 h prior to imaging.

**Scratch-wound image analysis:** For image analysis, cells were identified through a series of filters applied to individual images using Python, which produced binary images. Adjacent frames were shifted to maximize the total overlap in the binary images and cells were assigned to tracks based on maximum overlap. Cells unaccounted for by this method were assigned tracks by minimizing the centroid displacement between remaining cells. Edge cells were identified as being within 75  $\mu\text{m}$  of the migratory front. Loose and bulk cells were identified by their position relative to the migratory front and edge cells. Instantaneous centroid velocities were used for further analysis. Cell tracks that were detected in a minimum of 10 frames were analyzed.

**Cell-cell junction remodeling assay:** For mature AJ remodeling assays,  $5 \times 10^4$  cells were plated in 6-well tissue culture treated dishes and allowed to form small colonies (<40 cells). The cells were treated with MRC-5 conditioned media, and imaged every 5

minutes. Images were taken with a Nikon Eclipse TE2000-U inverted microscope and CoolSnap ES CCD camera.

**Invasion Assay:** For invasion assays, tumor spheroids formed by the hanging drop method were isolated 96 hours after suspension culture, and embedded in a Collagen I matrix (2mg/mL). The Collagen I matrix was allowed to solidify for 90 minutes prior to being overlaid with 10% FBS containing DMEM with 50 ng/mL HGF. Additionally, the tumor spheroids were treated with vehicle control (DMSO). The invasion occurred over 8 days.

**Soft agar colony formation assay:** First a layer of 0.5% agarose-containing DMEM was solidified at the bottom of wells of 6-well dishes to prevent cells from attaching. Cells were mixed into liquid 0.33% agarose at the desired cell numbers and allowed to solidify on top of the 0.5% layer. For HT-29/19A cells 500 cells were used. Colonies greater than 0.05 $\mu\text{m}^2$  in area were counted.

**Mice:** NOD-*scid* IL2R $\gamma^{\text{null}}$  mice (NSG) (Jackson Laboratory, Bar Harbor, ME) were injected subcutaneously with  $2 \times 10^6$  Scr and shF cells and intra-splenic with  $1 \times 10^6$  Scr and shF cells. Three weeks' post-injection primary and secondary tumors were excised and measured.

**Zebrafish metastasis assay:** Zebrafish (*Danio rerio*) were reared and maintained at 28.5°C. *Tg(kdrl:EGFP)mitfa<sup>b692/b692</sup>* was generated by crossing *Tg(kdrl:EGFP)* with *mitfa<sup>b692/b692</sup>* (Zebrafish International Resource Center, Eugene, OR). 300-500 HT-29/19A

Scr and HT-29/19A-shF cells labeled with CM-Dil (ThermoFisher) were microinjected into yolk sac of 2-day old embryos using a pressure injector (Harvard Apparatus, Holliston, MA) and manipulator (MM33-Righ, Märzhäuser Wetzlar, Germany). Embryos and cells injected in the yolk were incubated at 34°C and imaged using OLYMPUS IX51 fluorescence microscope, OLYMPUS XM10 camera and cellSens Dimension software (Olympus, Center Valley, PA, USA).

**Immunofluorescence and live cell fluorescence microscopy:** Confocal images were acquired using the Olympus FV2000 inverted confocal microscope. Unless otherwise indicated all data were obtained by performing three independent experiments with  $n = 10$  fields/group and  $>300$  cells/group were analyzed each time. Nuclei were counter stained with DAPI. Tumor spheroids were studied in three independent experiments with 10 spheroids per group in each experiment. Plot profiles were generated by measuring the distribution of AJ associated proteins in regions of interest (ROI) highlighted by a white line, 10  $\mu\text{m}$  long.

**Chromatin Immunoprecipitation.** ChIP was carried out as previously described.(Bado et al., 2016) Briefly, cells were fixed with 1.5% paraformaldehyde, lysed, nuclei were purified, and then chromatin was sheared by sonification. Immunoprecipitation was carried out with  $\beta$ -catenin monoclonal antibody and Protein G magnetic beads (Sigma-Aldrich). For PCR, the following primers were used:

MMP9:

F: 5'-CCTCCTTAAAGCCCCCACAA-3',

R: 5'-CAGTCCACCCTTGTGCTCTT-3';

CCND1:

F: 5'-CAGAAGAGCGCGAGGGAG-3',

R: 5'-ATGGAACACCAGCTCCTGTG;

MYC,

F: 5'-GAGGCGAACACACAACGTCTT-3',

R: 5'-CGCAACAAGTCCTCTTCAGAAA-3'

MMP9 negative control,

F: 5'-GTGGGACCTCAACGTCTGTC-3',

R: 5'- CACCACCTCTAAGCACTGACAT-3'.

Fascin1:

F: 5'-AGGCGGCCAACGAGAGGAAC-3'

R: 5'-ACGATGATGGGGCGGTTGAT'3'

CD44:

F:5'-GCAGTCAACAGTCGAAGAAGG'3'

R: 5'-TGTCTCCACAGCTCCATT-3'

MMP7:

F:5'-CTTACCTCGGATCGTAGTGG-3'

R: 5'-CCCCAACTAACCCTCTTGAAGT-3'

AXIN2:

F:5'-AACCTATGCCCCGTTTCCTCTA-3'

R:5'-GAGTGTAAGACTTGGTCCACC-3'

TCF1:

F:5'-CCAGTGTGCACCCTTCCTAT-3'

R:5'-AGCCCCACAGAGAACTGAA-3'

**Promoter reporter assays. Promoter reporter assays.** Cells were transfected in 24-well dishes using Lipofectamine 2000 (ThermoFisher) with  $\beta$ -catenin reporter Super 8X TOPFlash and pSV- $\beta$ -Galactosidase control vector. All cells were lysed approximately 24 hours post-transfection, and luciferase activity was measured with Luciferase Assay (Promega, Madison, Wisconsin, USA) and  $\beta$ -Galactosidase with chlorophenol red- $\beta$ -D-galactopyranoside (CPRG). Reporter activity was normalized to  $\beta$ -Galactosidase activity. 24 hours' post-transfection, cells were treated with DMSO, 20 $\mu$ M G2, or 100 $\mu$ M G2 for 24 hours. Luminescence was quantified with VICTOR Multilabel Plate Reader (PerkinElmer, Waltham, MA, USA).

**Fascin1 and  $\beta$ -catenin immunohistochemistry scoring:** Patient tumor microarrays were immunostained for fascin1 and total  $\beta$ -catenin. Fascin1 was scored using the method of Hashimoto *et al* and  $\beta$ -catenin was scored by adapting the method of Hugh *et al*. (Hashimoto *et al.*, 2006; Hugh *et al.*, 1999) Immunohistology in paired tumor panels show expression of fascin1 and  $\beta$ -catenin in the same tumor.

**Statistical Analysis:** Data are expressed as mean  $\pm$  standard deviation (SD) or  $\pm$  standard error (SE). Significance was determined by Student's t-test, Mann-Whitney U test, Kuiper's test, or Watson U2 test.

**Study approval:** All animal studies were performed in accordance with animal protocols approved by the University of Houston Institutional Animal Care and Use Committee.

## References Cited

- Ashktorab, H., Delker, D., Kanth, P., Goel, A., Carethers, J.M., and Brim, H. (2019). Molecular Characterization of Sessile Serrated Adenoma/Polyps From a Large African American Cohort. *Gastroenterology* 157, 572-574. 10.1053/j.gastro.2019.04.015.
- Ayollo, D.V., Zhitnyak, I.Y., Vasiliev, J.M., and Gloushankova, N.A. (2009). Rearrangements of the actin cytoskeleton and E-cadherin-based adherens junctions caused by neoplastic transformation change cell-cell interactions. *PLoS One* 4, e8027. 10.1371/journal.pone.0008027.
- Bado, I., Nikolos, F., Rajapaksa, G., Gustafsson, J.A., and Thomas, C. (2016). ERbeta decreases the invasiveness of triple-negative breast cancer cells by regulating mutant p53 oncogenic function. *Oncotarget* 7, 13599-13611. 10.18632/oncotarget.7300.
- Barnawi, R., Al-Khaldi, S., Majed Sleiman, G., Sarkar, A., Al-Dhfyan, A., Al-Mohanna, F., Ghebeh, H., and Al-Alwan, M. (2016). Fascin Is Critical for the Maintenance of Breast Cancer Stem Cell Pool Predominantly via the Activation of the Notch Self-Renewal Pathway. *Stem Cells* 34, 2799-2813. 10.1002/stem.2473.
- Baum, B., and Georgiou, M. (2011). Dynamics of adherens junctions in epithelial establishment, maintenance, and remodeling. *J Cell Biol* 192, 907-917. 10.1083/jcb.201009141.
- Benham-Pyle, B.W., Pruitt, B.L., and Nelson, W.J. (2015). Cell adhesion. Mechanical strain induces E-cadherin-dependent Yap1 and beta-catenin activation to drive cell cycle entry. *Science* 348, 1024-1027. 10.1126/science.aaa4559.
- Chen, B., Scurrah, C.R., McKinley, E.T., Simmons, A.J., Ramirez-Solano, M.A., Zhu, X., Markham, N.O., Heiser, C.N., Vega, P.N., Rolong, A., et al. (2021). Differential pre-

malignant programs and microenvironment chart distinct paths to malignancy in human colorectal polyps. *Cell* 184, 6262-6280 e6226. 10.1016/j.cell.2021.11.031.

Cohan, C.S., Welnhof, E.A., Zhao, L., Matsumura, F., and Yamashiro, S. (2001). Role of the actin bundling protein fascin in growth cone morphogenesis: localization in filopodia and lamellipodia. *Cell Motil Cytoskeleton* 48, 109-120. 10.1002/1097-0169(200102)48:2<109::AID-CM1002>3.0.CO;2-G.

Conesa-Zamora, P., Garcia-Solano, J., Garcia-Garcia, F., Turpin Mdel, C., Trujillo-Santos, J., Torres-Moreno, D., Oviedo-Ramirez, I., Carbonell-Munoz, R., Munoz-Delgado, E., Rodriguez-Braun, E., et al. (2013). Expression profiling shows differential molecular pathways and provides potential new diagnostic biomarkers for colorectal serrated adenocarcinoma. *Int J Cancer* 132, 297-307. 10.1002/ijc.27674.

De Sousa, E.M.F., Wang, X., Jansen, M., Fessler, E., Trinh, A., de Rooij, L.P., de Jong, J.H., de Boer, O.J., van Leersum, R., Bijlsma, M.F., et al. (2013). Poor-prognosis colon cancer is defined by a molecularly distinct subtype and develops from serrated precursor lesions. *Nat Med* 19, 614-618. 10.1038/nm.3174.

Desai, R., Sarpal, R., Ishiyama, N., Pellikka, M., Ikura, M., and Tepass, U. (2013). Monomeric alpha-catenin links cadherin to the actin cytoskeleton. *Nat Cell Biol* 15, 261-273. 10.1038/ncb2685.

Fernandez-Sanchez, M.E., Barbier, S., Whitehead, J., Bealle, G., Michel, A., Latorre-Ossa, H., Rey, C., Fouassier, L., Claperon, A., Brulle, L., et al. (2015). Mechanical induction of the tumorigenic beta-catenin pathway by tumour growth pressure. *Nature* 523, 92-95. 10.1038/nature14329.

- Freedman, S.L., Suarez, C., Winkelman, J.D., Kovar, D.R., Voth, G.A., Dinner, A.R., and Hocky, G.M. (2019). Mechanical and kinetic factors drive sorting of F-actin cross-linkers on bundles. *Proc Natl Acad Sci U S A* 116, 16192-16197. 10.1073/pnas.1820814116.
- George, S.P., Chen, H., Conrad, J.C., and Khurana, S. (2013). Regulation of directional cell migration by membrane-induced actin bundling. *J Cell Sci* 126, 312-326. 10.1242/jcs.116244.
- Gloushankova, N.A., Rubtsova, S.N., and Zhitnyak, I.Y. (2017). Cadherin-mediated cell-cell interactions in normal and cancer cells. *Tissue Barriers* 5, e1356900. 10.1080/21688370.2017.1356900.
- Hashimoto, Y., Skacel, M., Lavery, I.C., Mukherjee, A.L., Casey, G., and Adams, J.C. (2006). Prognostic significance of fascin expression in advanced colorectal cancer: an immunohistochemical study of colorectal adenomas and adenocarcinomas. *BMC Cancer* 6, 241. 1471-2407-6-241 [pii]10.1186/1471-2407-6-241.
- Herr, R., Kohler, M., Androva, H., Weinberg, F., Moller, Y., Halbach, S., Lutz, L., Mastroianni, J., Klose, M., Bittermann, N., et al. (2015). B-Raf inhibitors induce epithelial differentiation in BRAF-mutant colorectal cancer cells. *Cancer Res* 75, 216-229. 10.1158/0008-5472.CAN-13-3686.
- Hoffman, B.D., and Yap, A.S. (2015). Towards a Dynamic Understanding of Cadherin-Based Mechanobiology. *Trends Cell Biol* 25, 803-814. 10.1016/j.tcb.2015.09.008.
- Hugh, T.J., Dillon, S.A., Taylor, B.A., Pignatelli, M., Poston, G.J., and Kinsella, A.R. (1999). Cadherin-catenin expression in primary colorectal cancer: a survival analysis. *Br J Cancer* 80, 1046-1051. 10.1038/sj.bjc.6690461.

Humtsoe, J.O., Koya, E., Pham, E., Aramoto, T., Zuo, J., Ishikawa, T., and Kramer, R.H. (2012). Transcriptional profiling identifies upregulated genes following induction of epithelial-mesenchymal transition in squamous carcinoma cells. *Exp Cell Res* 318, 379-390. 10.1016/j.yexcr.2011.11.011.

Jia, D., Jolly, M.K., Tripathi, S.C., Den Hollander, P., Huang, B., Lu, M., Celiktaş, M., Ramirez-Pena, E., Ben-Jacob, E., Onuchic, J.N., et al. (2017). Distinguishing mechanisms underlying EMT tristability. *Cancer Conver* 1, 2. 10.1186/s41236-017-0005-8.

Jolly, M.K., Tripathi, S.C., Jia, D., Mooney, S.M., Celiktaş, M., Hanash, S.M., Mani, S.A., Pienta, K.J., Ben-Jacob, E., and Levine, H. (2016). Stability of the hybrid epithelial/mesenchymal phenotype. *Oncotarget* 7, 27067-27084. 10.18632/oncotarget.8166.

Kanth, P., Boylan, K.E., Bronner, M.P., Boucher, K.M., Hazel, M.W., Yao, R., Pop, S., Bernard, P.S., and Delker, D.A. (2019). Molecular Biomarkers of Sessile Serrated Adenoma/Polyps. *Clin Transl Gastroenterol* 10, e00104. 10.14309/ctg.0000000000000104.

Kanth, P., Bronner, M.P., Boucher, K.M., Burt, R.W., Neklason, D.W., Hagedorn, C.H., and Delker, D.A. (2016). Gene Signature in Sessile Serrated Polyps Identifies Colon Cancer Subtype. *Cancer Prev Res (Phila)* 9, 456-465. 10.1158/1940-6207.CAPR-15-0363.

Kopetz, S., Desai, J., Chan, E., Hecht, J.R., O'Dwyer, P.J., Maru, D., Morris, V., Janku, F., Dasari, A., Chung, W., et al. (2015). Phase II Pilot Study of Vemurafenib in Patients

With Metastatic BRAF-Mutated Colorectal Cancer. *J Clin Oncol* 33, 4032-4038. 10.1200/JCO.2015.63.2497.

Kopetz, S., Grothey, A., Yaeger, R., Van Cutsem, E., Desai, J., Yoshino, T., Wasan, H., Ciardiello, F., Loupakis, F., Hong, Y.S., et al. (2019). Encorafenib, Binimetinib, and Cetuximab in BRAF V600E-Mutated Colorectal Cancer. *N Engl J Med* 381, 1632-1643. 10.1056/NEJMoa1908075.

Krendel, M., Gloushankova, N.A., Bonder, E.M., Feder, H.H., Vasiliev, J.M., and Gelfand, I.M. (1999). Myosin-dependent contractile activity of the actin cytoskeleton modulates the spatial organization of cell-cell contacts in cultured epitheliocytes. *Proc Natl Acad Sci U S A* 96, 9666-9670. 10.1073/pnas.96.17.9666.

le Duc, Q., Shi, Q., Blonk, I., Sonnenberg, A., Wang, N., Leckband, D., and de Rooij, J. (2010). Vinculin potentiates E-cadherin mechanosensing and is recruited to actin-anchored sites within adherens junctions in a myosin II-dependent manner. *J Cell Biol* 189, 1107-1115. 10.1083/jcb.201001149.

Le, S., Hu, X., Yao, M., Chen, H., Yu, M., Xu, X., Nakazawa, N., Margadant, F.M., Sheetz, M.P., and Yan, J. (2017). Mechanotransmission and Mechanosensing of Human alpha-Actinin 1. *Cell Rep* 21, 2714-2723. 10.1016/j.celrep.2017.11.040.

Li, A., Morton, J.P., Ma, Y., Karim, S.A., Zhou, Y., Faller, W.J., Woodham, E.F., Morris, H.T., Stevenson, R.P., Juin, A., et al. (2014). Fascin is regulated by slug, promotes progression of pancreatic cancer in mice, and is associated with patient outcomes. *Gastroenterology* 146, 1386-1396 e1381-1317. 10.1053/j.gastro.2014.01.046.

Li, J.X.H., Tang, V.W., and Brieher, W.M. (2020). Actin protrusions push at apical junctions to maintain E-cadherin adhesion. *Proc Natl Acad Sci U S A* *117*, 432-438. 10.1073/pnas.1908654117.

Lin, S., Taylor, M.D., Singh, P.K., and Yang, S. (2021). How does fascin promote cancer metastasis? *FEBS J* *288*, 1434-1446. 10.1111/febs.15484.

Makrodouli, E., Oikonomou, E., Koc, M., Andera, L., Sasazuki, T., Shirasawa, S., and Pintzas, A. (2011). BRAF and RAS oncogenes regulate Rho GTPase pathways to mediate migration and invasion properties in human colon cancer cells: a comparative study. *Mol Cancer* *10*, 118. 10.1186/1476-4598-10-118.

Mathew, S., George, S.P., Wang, Y., Siddiqui, M.R., Srinivasan, K., Tan, L., and Khurana, S. (2008). Potential molecular mechanism for c-Src kinase-mediated regulation of intestinal cell migration. *J Biol Chem* *283*, 22709-22722. 10.1074/jbc.M801319200.

Michael, M., and Yap, A.S. (2013). The regulation and functional impact of actin assembly at cadherin cell-cell adhesions. *Semin Cell Dev Biol* *24*, 298-307. 10.1016/j.semcdb.2012.12.004.

Naphade, S., Sharma, J., Gaide Chevronnay, H.P., Shook, M.A., Yeagy, B.A., Rocca, C.J., Ur, S.N., Lau, A.J., Courtoy, P.J., and Cherqui, S. (2015). Brief reports: Lysosomal cross-correction by hematopoietic stem cell-derived macrophages via tunneling nanotubes. *Stem Cells* *33*, 301-309. 10.1002/stem.1835.

Niewiadomska, P., Godt, D., and Tepass, U. (1999). DE-Cadherin is required for intercellular motility during *Drosophila* oogenesis. *J Cell Biol* *144*, 533-547. 10.1083/jcb.144.3.533.

Osswald, M., Jung, E., Sahm, F., Solecki, G., Venkataramani, V., Blaes, J., Weil, S., Horstmann, H., Wiestler, B., Syed, M., et al. (2015). Brain tumour cells interconnect to a functional and resistant network. *Nature* 528, 93-98. 10.1038/nature16071.

Pai, R.K., Jayachandran, P., Koong, A.C., Chang, D.T., Kwok, S., Ma, L., Arber, D.A., Balise, R.R., Tubbs, R.R., Shadrach, B., and Pai, R.K. (2012). BRAF-mutated, microsatellite-stable adenocarcinoma of the proximal colon: an aggressive adenocarcinoma with poor survival, mucinous differentiation, and adverse morphologic features. *Am J Surg Pathol* 36, 744-752. 10.1097/PAS.0b013e31824430d7.

Patnaik, S., George, S.P., Pham, E., Roy, S., Singh, K., Mariadason, J.M., and Khurana, S. (2016). By moonlighting in the nucleus, villin regulates epithelial plasticity. *Mol Biol Cell* 27, 535-548. 10.1091/mbc.E15-06-0453.

Poznansky, M.C., Olszak, I.T., Foxall, R., Evans, R.H., Luster, A.D., and Scadden, D.T. (2000). Active movement of T cells away from a chemokine. *Nat Med* 6, 543-548. 10.1038/75022.

Przybyla, L., Lakins, J.N., and Weaver, V.M. (2016). Tissue Mechanics Orchestrate Wnt-Dependent Human Embryonic Stem Cell Differentiation. *Cell Stem Cell* 19, 462-475. 10.1016/j.stem.2016.06.018.

Reischmann, N., Andrieux, G., Griffin, R., Reinheckel, T., Boerries, M., and Brummer, T. (2020). BRAF(V600E) drives dedifferentiation in small intestinal and colonic organoids and cooperates with mutant p53 and Apc loss in transformation. *Oncogene* 39, 6053-6070. 10.1038/s41388-020-01414-9.

Riemer, P., Sreekumar, A., Reinke, S., Rad, R., Schafer, R., Sers, C., Blaker, H., Herrmann, B.G., and Morkel, M. (2015). Transgenic expression of oncogenic BRAF

induces loss of stem cells in the mouse intestine, which is antagonized by beta-catenin activity. *Oncogene* 34, 3164-3175. 10.1038/onc.2014.247.

Ristic, B., Kopel, J., Sherazi, S.A.A., Gupta, S., Sachdeva, S., Bansal, P., Ali, A., Perisetti, A., and Goyal, H. (2021). Emerging Role of Fascin-1 in the Pathogenesis, Diagnosis, and Treatment of the Gastrointestinal Cancers. *Cancers (Basel)* 13 (1), 2536. 10.3390/cancers13112536.

Roper, J.C., Mitrossilis, D., Stirnemann, G., Waharte, F., Brito, I., Fernandez-Sanchez, M.E., Baaden, M., Salamero, J., and Farge, E. (2018). The major beta-catenin/E-cadherin junctional binding site is a primary molecular mechano-transducer of differentiation in vivo. *Elife* 7, e33381. 10.7554/eLife.33381.

Rustom, A., Saffrich, R., Markovic, I., Walther, P., and Gerdes, H.H. (2004). Nanotubular highways for intercellular organelle transport. *Science* 303, 1007-1010.

Schnittler, H., Taha, M., Schnittler, M.O., Taha, A.A., Lindemann, N., and Seebach, J. (2014). Actin filament dynamics and endothelial cell junctions: the Ying and Yang between stabilization and motion. *Cell Tissue Res* 355, 529-543. 10.1007/s00441-014-1856-2.

Schoumacher, M., El-Marjou, F., Lae, M., Kambou, N., Louvard, D., Robine, S., and Vignjevic, D.M. (2014). Conditional expression of fascin increases tumor progression in a mouse model of intestinal cancer. *Eur J Cell Biol* 93, 388-395. 10.1016/j.ejcb.2014.08.002.

Seddiki, R., Narayana, G., Strale, P.O., Balcioglu, H.E., Peyret, G., Yao, M., Le, A.P., Teck Lim, C., Yan, J., Ladoux, B., and Mege, R.M. (2018). Force-dependent binding of

vinculin to alpha-catenin regulates cell-cell contact stability and collective cell behavior. *Mol Biol Cell* 29, 380-388. 10.1091/mbc.E17-04-0231.

Taguchi, K., Ishiuchi, T., and Takeichi, M. (2011). Mechanosensitive EPLIN-dependent remodeling of adherens junctions regulates epithelial reshaping. *J Cell Biol* 194, 643-656. 10.1083/jcb.201104124.

Tampakis, A., Tampaki, E.C., Nonni, A., Kostakis, I.D., Posabella, A., Kontzoglou, K., von Flue, M., Felekouras, E., Kouraklis, G., and Nikiteas, N. (2021). High fascin-1 expression in colorectal cancer identifies patients at high risk for early disease recurrence and associated mortality. *BMC Cancer* 21, 153. 10.1186/s12885-021-07842-4.

Tan, V.Y., Lewis, S.J., Adams, J.C., and Martin, R.M. (2013). Association of fascin-1 with mortality, disease progression and metastasis in carcinomas: a systematic review and meta-analysis. *BMC Med* 11, 52. 10.1186/1741-7015-11-52.

Tebbutt, N.C., Wilson, K., GebSKI, V.J., Cummins, M.M., Zannino, D., van Hazel, G.A., Robinson, B., Broad, A., Ganju, V., Ackland, S.P., et al. (2010). Capecitabine, bevacizumab, and mitomycin in first-line treatment of metastatic colorectal cancer: results of the Australasian Gastrointestinal Trials Group Randomized Phase III MAX Study. *J Clin Oncol* 28, 3191-3198. JCO.2009.27.7723 [pii]10.1200/JCO.2009.27.7723.

Tong, K., Pellon-Cardenas, O., Siriachai, V.R., Warder, B.N., Kothari, O.A., Perekatt, A.O., Fokas, E.E., Fullem, R.L., Zhou, A., Thackray, J.K., et al. (2017). Degree of Tissue Differentiation Dictates Susceptibility to BRAF-Driven Colorectal Cancer. *Cell Rep* 21, 3833-3845. 10.1016/j.celrep.2017.11.104.

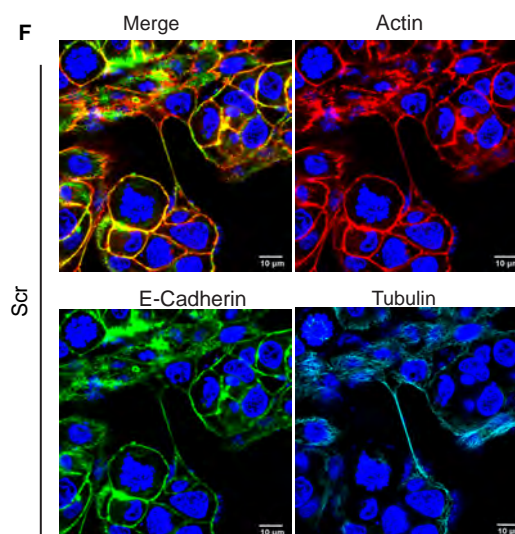
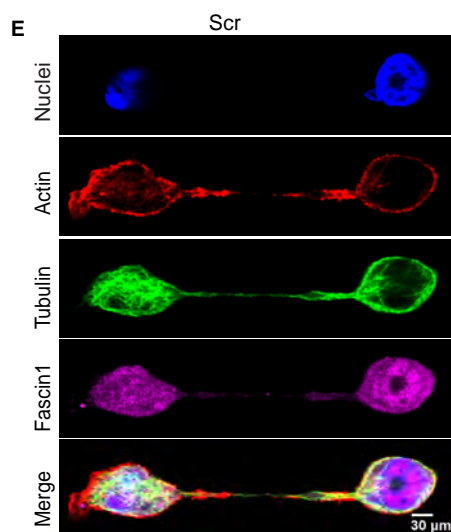
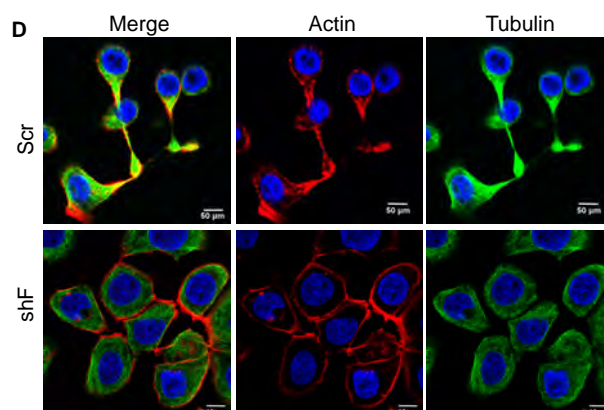
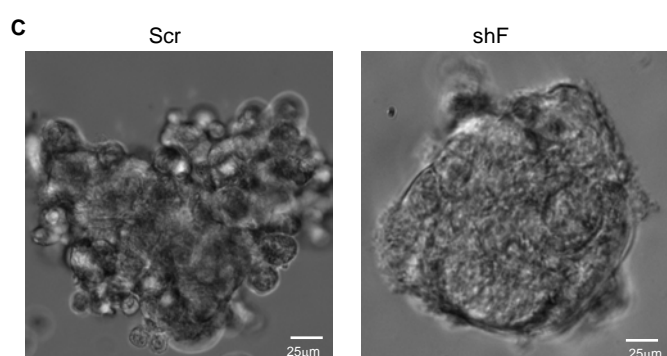
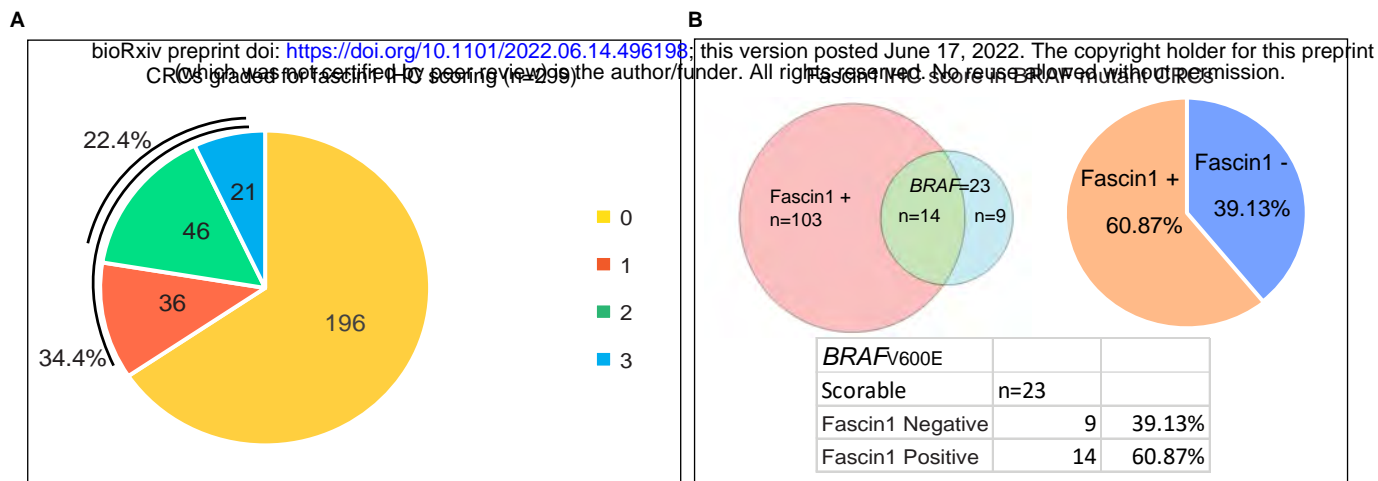
- Vianello, F., Olszak, I.T., and Poznansky, M.C. (2005). Fugetaxis: active movement of leukocytes away from a chemokinetic agent. *J Mol Med (Berl)* 83, 752-763. 10.1007/s00109-005-0675-z.
- Vignjevic, D., Schoumacher, M., Gavert, N., Janssen, K.P., Jih, G., Lae, M., Louvard, D., Ben-Ze'ev, A., and Robine, S. (2007). Fascin, a novel target of beta-catenin-TCF signaling, is expressed at the invasive front of human colon cancer. *Cancer Res* 67, 6844-6853.
- Wang, Y., George, S.P., Roy, S., Pham, E., Esmaeilniakooshkghazi, A., and Khurana, S. (2016). Both the anti- and pro-apoptotic functions of villin regulate cell turnover and intestinal homeostasis. *Sci Rep* 6, 35491. 10.1038/srep35491.
- Whitehead, J., Vignjevic, D., Futterer, C., Beaurepaire, E., Robine, S., and Farge, E. (2008). Mechanical factors activate beta-catenin-dependent oncogene expression in APC mouse colon. *HFSP J* 2, 286-294. 10.2976/1.2955566.
- Winkelman, J.D., Suarez, C., Hocky, G.M., Harker, A.J., Morganthaler, A.N., Christensen, J.R., Voth, G.A., Bartles, J.R., and Kovar, D.R. (2016). Fascin- and alpha-Actinin-Bundled Networks Contain Intrinsic Structural Features that Drive Protein Sorting. *Curr Biol* 26, 2697-2706. 10.1016/j.cub.2016.07.080.
- Wu, J.M., Montgomery, E.A., and Iacobuzio-Donahue, C.A. (2008). Frequent beta-catenin nuclear labeling in sessile serrated polyps of the colorectum with neoplastic potential. *Am J Clin Pathol* 129, 416-423. 10.1309/603UQKM7C2KELGJU.
- Yachida, S., Mudali, S., Martin, S.A., Montgomery, E.A., and Iacobuzio-Donahue, C.A. (2009). Beta-catenin nuclear labeling is a common feature of sessile serrated adenomas

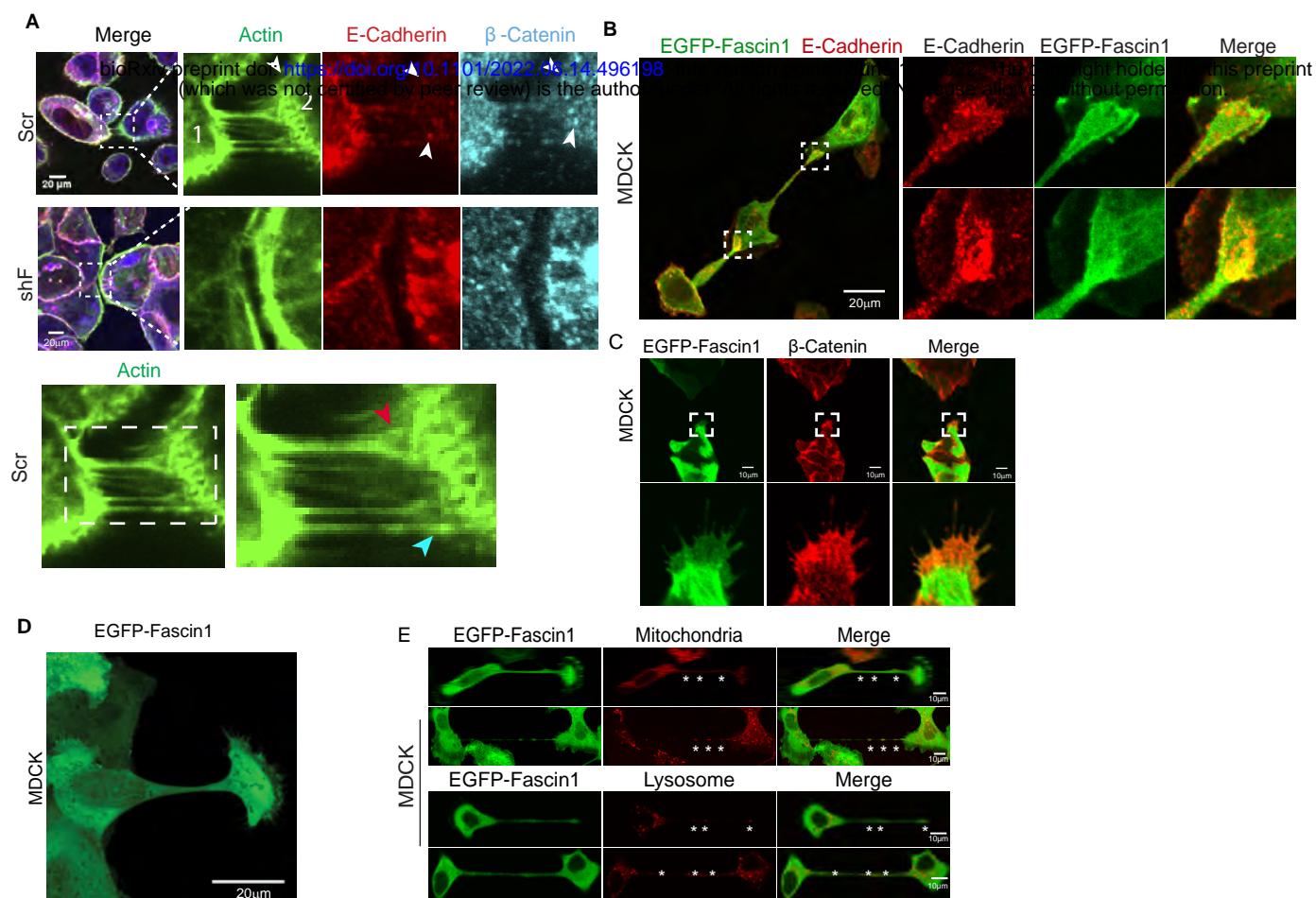
and correlates with early neoplastic progression after BRAF activation. *Am J Surg Pathol* 33, 1823-1832. 10.1097/PAS.0b013e3181b6da19.

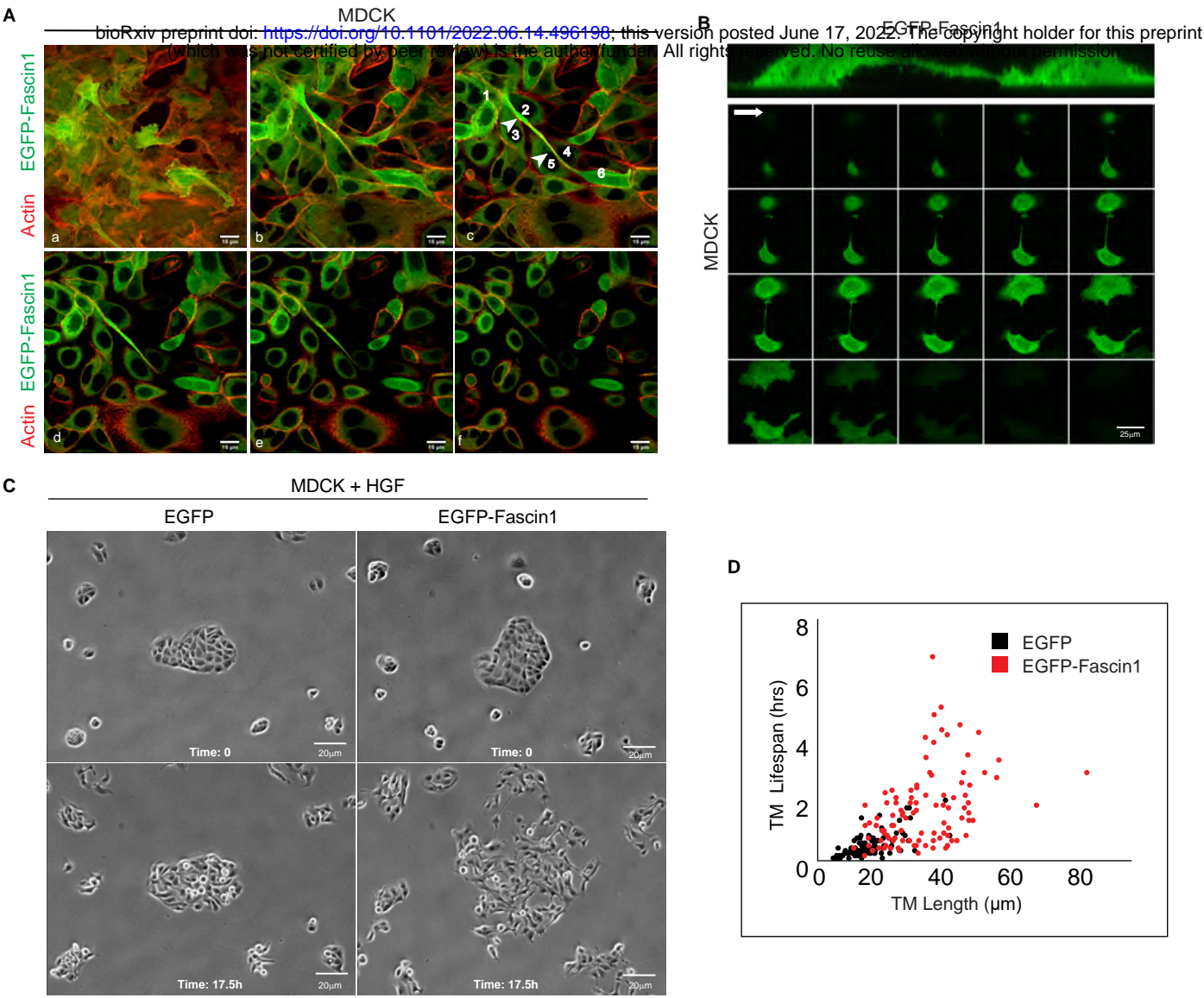
Yao, M., Qiu, W., Liu, R., Efremov, A.K., Cong, P., Seddiki, R., Payre, M., Lim, C.T., Ladoux, B., Mege, R.M., and Yan, J. (2014). Force-dependent conformational switch of alpha-catenin controls vinculin binding. *Nat Commun* 5, 4525. 10.1038/ncomms5525.

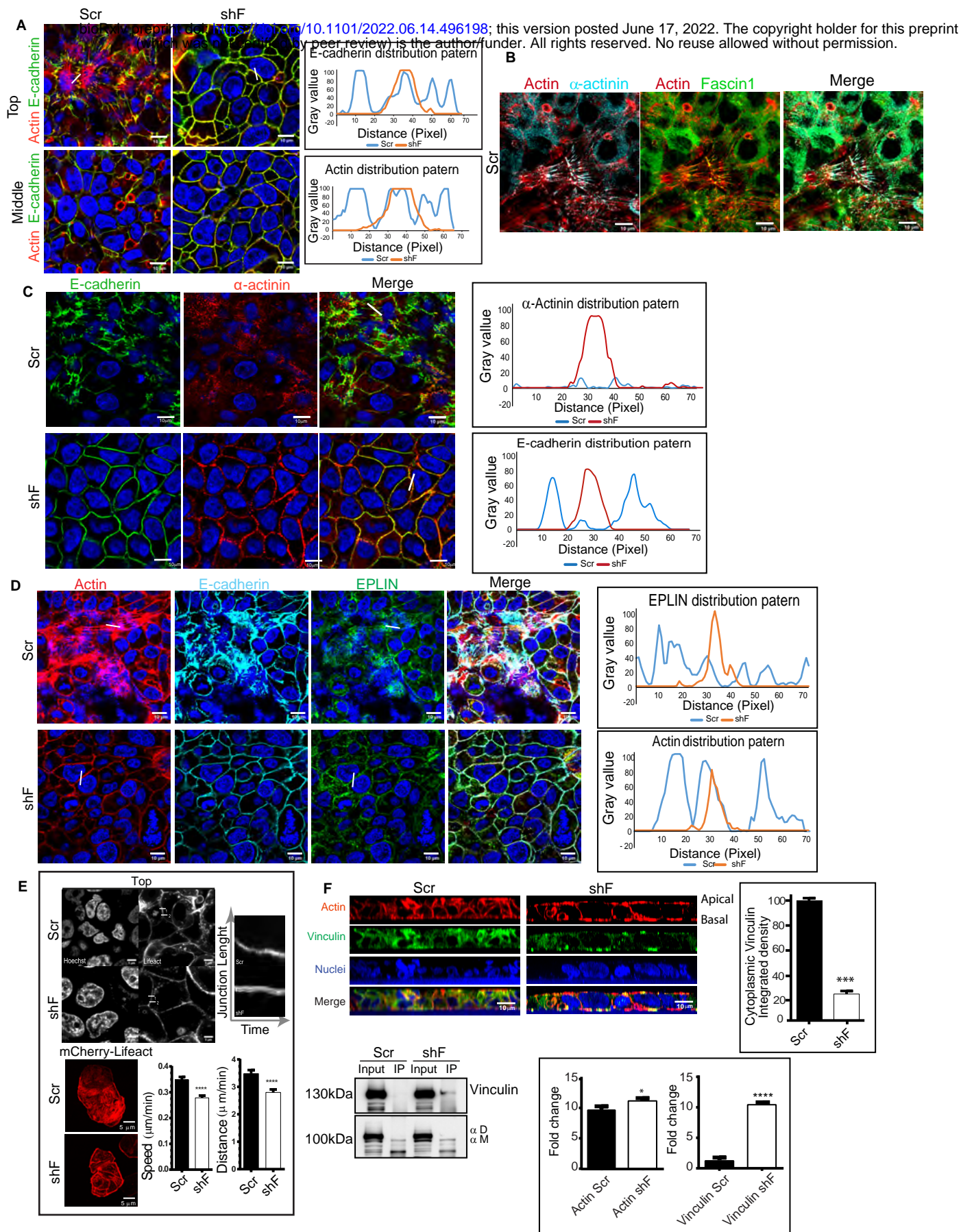
Yonemura, S. (2011). Cadherin-actin interactions at adherens junctions. *Curr Opin Cell Biol* 23, 515-522. 10.1016/j.ceb.2011.07.001.

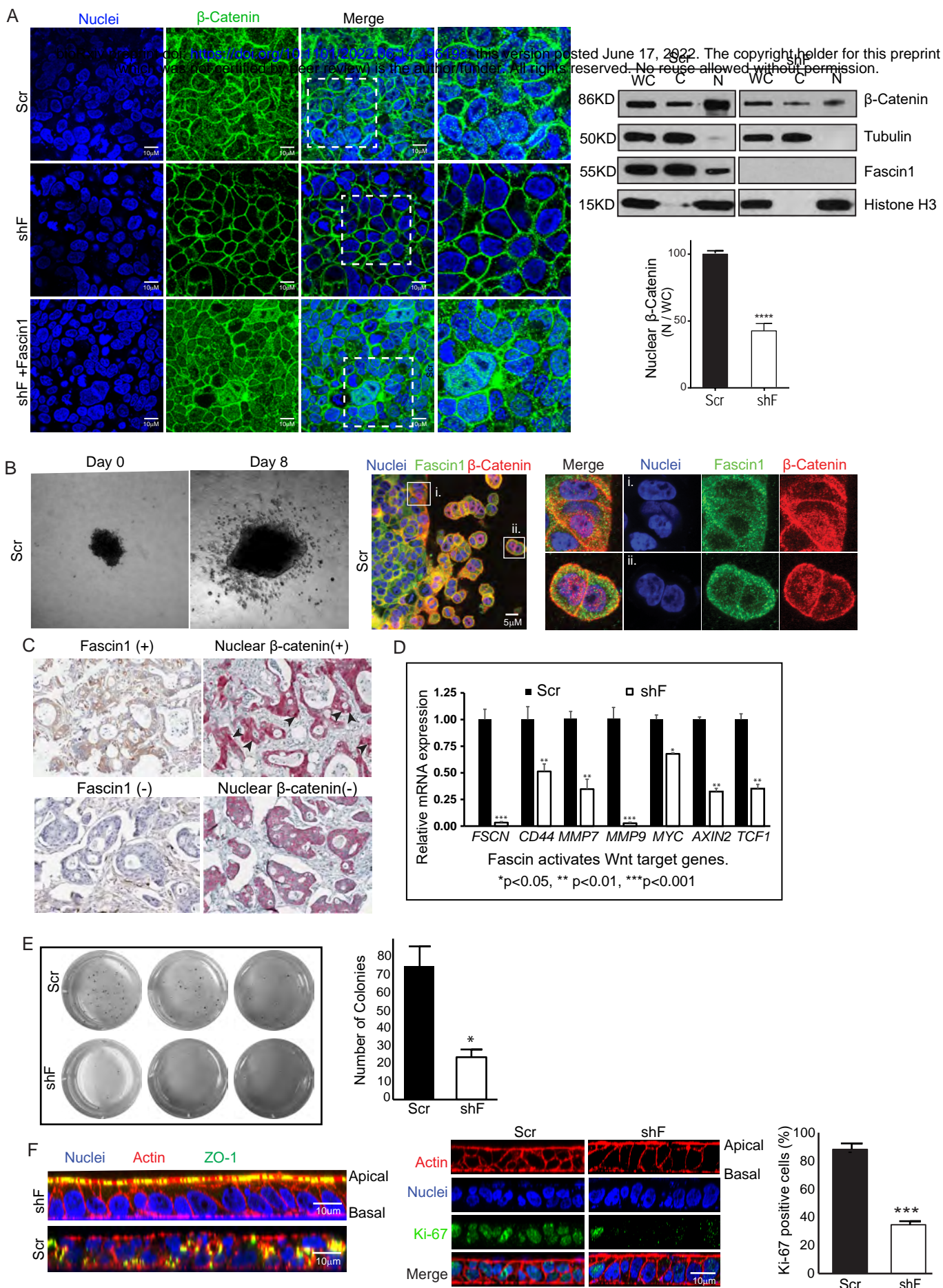
Yonemura, S., Wada, Y., Watanabe, T., Nagafuchi, A., and Shibata, M. (2010). alpha-Catenin as a tension transducer that induces adherens junction development. *Nat Cell Biol* 12, 533-542. 10.1038/ncb2055.

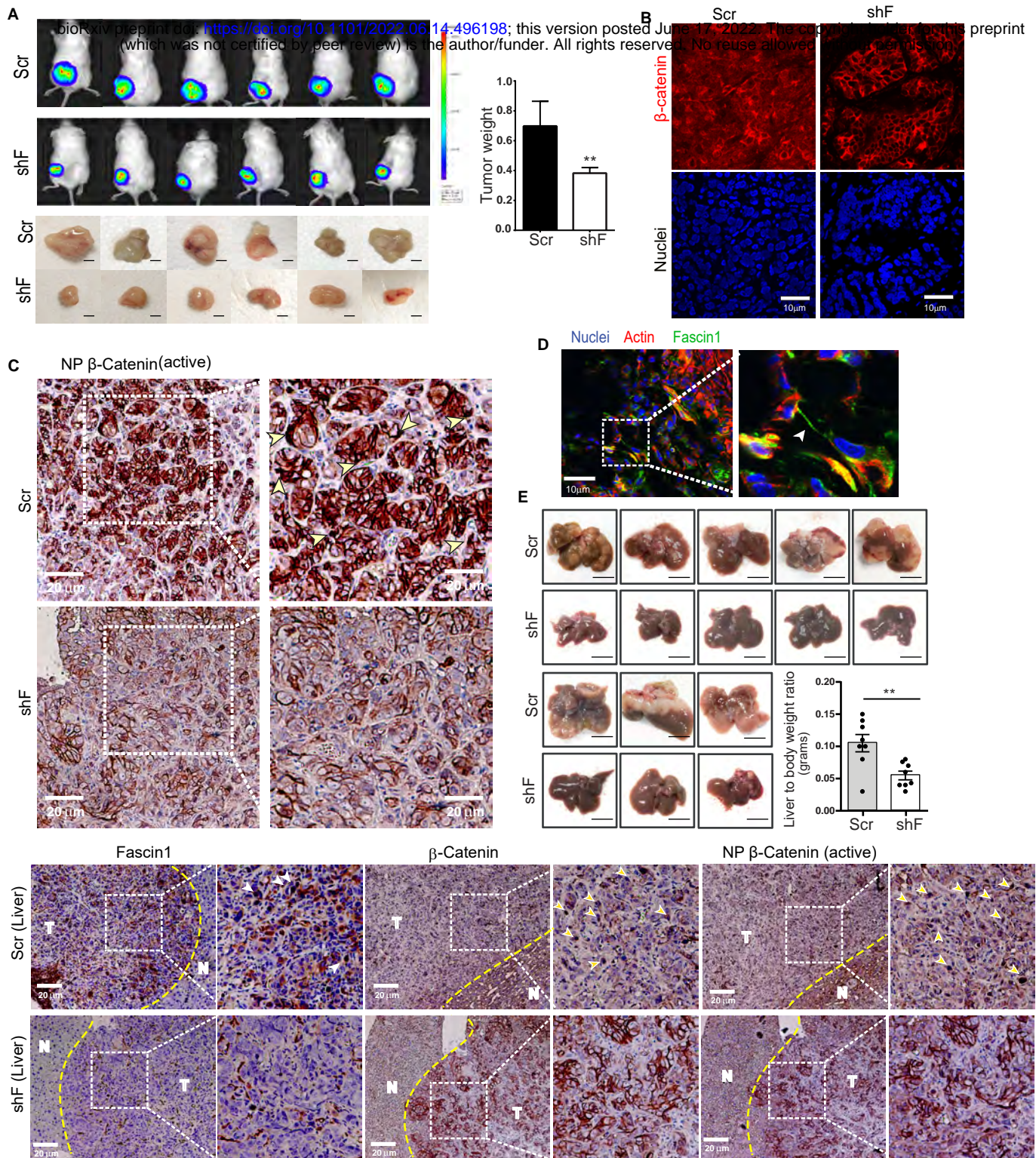




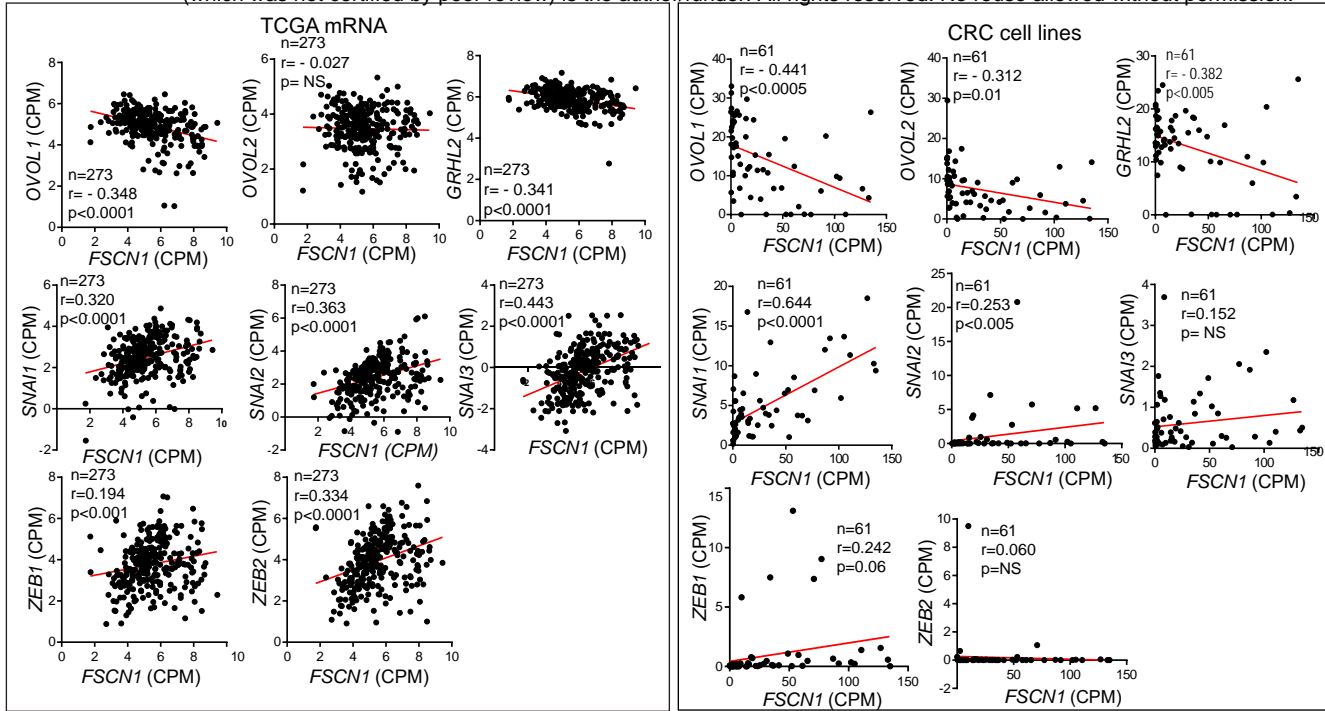




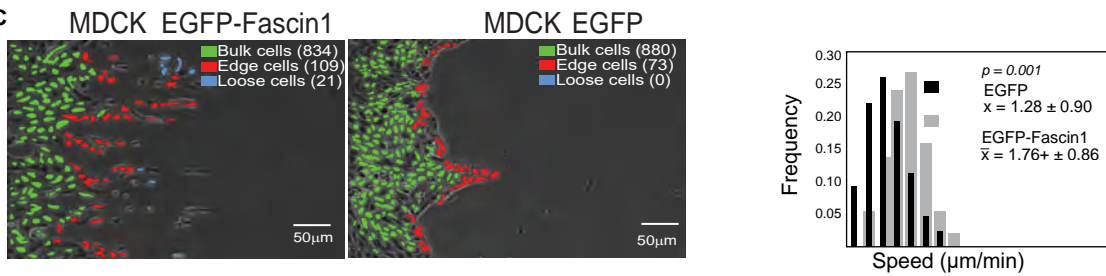




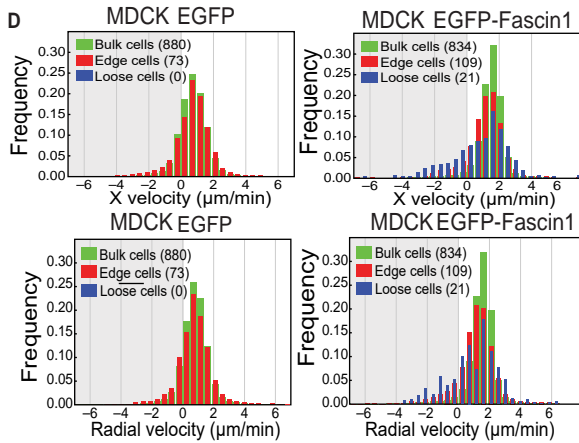
A



C



D



E

